Geophys. J. Int. (2006) doi: 10.1111/j.1365-246X.2006.03183.x

Balancing the plate motion budget in the South Island, New Zealand using GPS, geological and seismological data

Laura M. Wallace,[1] John Beavan,[1] Robert McCaffrey,[2] Kelvin Berryman[1] and Paul Denys[3]

[1]*GNS Science,* PO Box 30368, *Lower Hutt, New Zealand. E-mails: l.wallace@gns.cri.nz; j.beavan@gns.cri.nz; k.berryman@gns.cri.nz*
[2]*Department of Earth and Environmental Sciences, Rensselaer Polytechnic Inst, Troy, NY, USA. E-mail: mccafr@rpi.edu*
[3]*School of Surveying, University of Otago,* 310 *Castle St., Dunedin, New Zealand. E-mail: pdenys@stonebow.otago.ac.nz*

Accepted 2006 August 11. Received 2006 August 10; in original form 2005 November 1

SUMMARY

The landmass of New Zealand exists as a consequence of transpressional collision between the Australian and Pacific plates, providing an excellent opportunity to quantify the kinematics of deformation at this type of tectonic boundary. We interpret GPS, geological and seismological data describing the active deformation in the South Island, New Zealand by using an elastic, rotating block approach that automatically balances the Pacific/Australia relative plate motion budget. The data in New Zealand are fit to within uncertainty when inverted simultaneously for angular velocities of rotating tectonic blocks and the degree of coupling on faults bounding the blocks. We find that most of the plate motion budget has been accounted for in previous geological studies, although we suggest that the Porter's Pass/Amberley fault zone in North Canterbury, and a zone of faults in the foothills of the Southern Alps may have slip rates about twice that of the geological estimates. Up to 5 mm yr^{-1} of active deformation on faults distributed within the Southern Alps <100 km to the east of the Alpine Fault is possible. The role of tectonic block rotations in partitioning plate boundary deformation is less pronounced in the South Island compared to the North Island. Vertical axis rotation rates of tectonic blocks in the South Island are similar to that of the Pacific Plate, suggesting that edge forces dominate the block kinematics there. The southward migrating Chatham Rise exerts a major influence on the evolution of the New Zealand plate boundary; we discuss a model for the development of the Marlborough fault system and Hikurangi subduction zone in the context of this migration.

Key words: deformation, fault slip, geodynamics, GPS, New Zealand, tectonics.

1 INTRODUCTION

GPS-derived site velocities within wide-plate boundary zones help to quantify where strain is accumulating and how slip is partitioned in such zones. Accurate knowledge of the motion of the bounding plates from GPS-derived site velocities allows quantification of the total 'plate motion budget' that must be accommodated within the plate boundary zone. Unfortunately, it is not uncommon for multiple tectonic interpretations to fit the GPS data sets equally well at plate boundary zones (e.g. Wallace *et al.* 2004a). This non-uniqueness is due to trade-offs among the various sources of surface velocities in the plate boundary zone, and is particularly troublesome adjacent to subduction zones and in regions with many closely spaced active faults. However, when geodetic data from a plate boundary zone are interpreted in conjunction with Quaternary fault slip rates (from geological studies) and fault slip azimuth data (usually in the form of earthquake slip vectors), we can significantly narrow the range of viable kinematic models. An approach for integrating these datasets is to assess them in terms of rotating, elastic tectonic blocks (e.g. McCaffrey 1995, 2002). Fault slip rate and azimuth data provide information about the relative motion between the blocks (Morgan 1968) while GPS-derived site velocities provide information on rates, azimuths, reference frame, and interseismic coupling on faults bounding the blocks.

New Zealand, which occupies the boundary zone between the Pacific and Australian plates (Fig. 1), is well-suited for using GPS, geological, and earthquake slip vector data to study how plate boundary deformation is accommodated. Repeated campaign-style GPS measurements have been conducted at more than 800 points throughout the country since the early 1990's (e.g. Beavan *et al.* 1999; Beavan & Haines 2001; Darby & Beavan 2001; Wallace *et al.* 2004a, Fig. 2). Active faulting studies have been conducted for decades in New Zealand (e.g. Wellman 1953; Lensen 1968; Berryman *et al.* 1992; Van Dissen & Berryman 1996) and have yielded a comprehensive dataset of fault slip rates (GNS active faults database: http://data.gns.cri.nz/af/). Seismologists have utilized both historical data from earthquakes over the last 100 yr (e.g. Doser *et al.* 1999; Doser & Webb 2003), and modern data collected in the last 50 yr

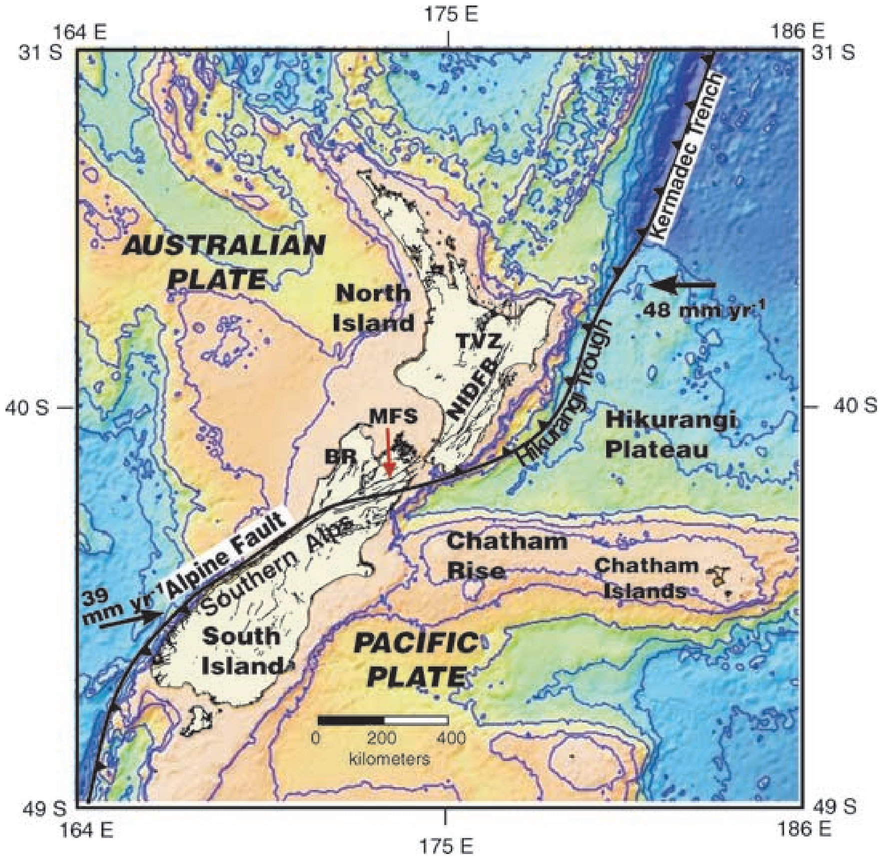

Figure 1. Regional tectonic setting of New Zealand (orange: shallow; blue: deep). MFS: Marlborough Fault System; NIDFB: North Island Dextral Fault Belt; TVZ; Taupo Volcanic Zone; BR denotes approximate location of shortening-related faults of the Buller region. Thin, black lines in the onland portion are active fault traces. Black arrows show Pacific/Australia relative convergence (e.g. Beavan *et al.* 2002).

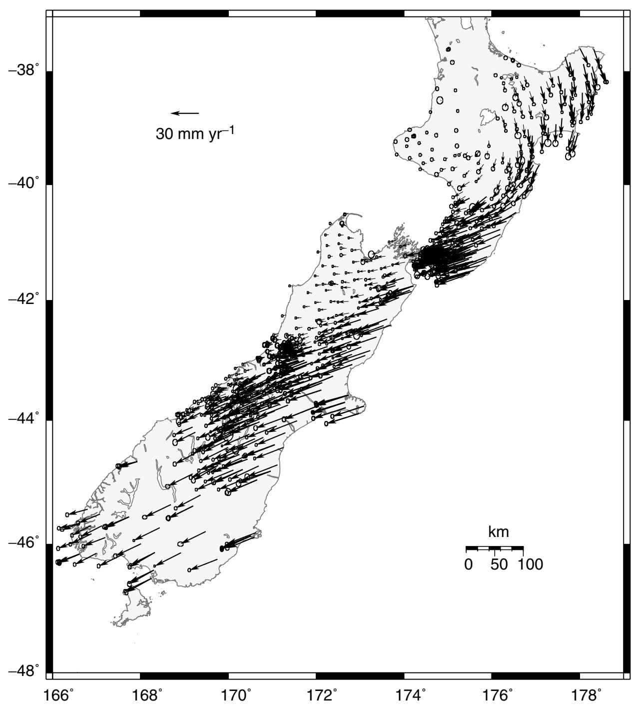

Figure 2. Velocities at GPS observation points in New Zealand, relative to the Australian Plate. Uncertainty ellipses are at 95 per cent confidence level.

(e.g. Anderson *et al.* 1993; Webb & Anderson 1998) to estimate earthquake source parameters for seismic events occurring in New Zealand.

As in our interpretation of the GPS velocity field and other data from the North Island (Wallace *et al.* 2004a), we use the elastic, rotating block approach (e.g. McCaffrey 2002) to integrate GPS, geological, and seismological data from the South Island of New Zealand. We include the Pacific-Australian relative plate motion (Beavan *et al.* 2002) as a fixed boundary condition in our kinematic model. We then use the model to quantify possible rates of faulting in regions where fault slip rates are not well-known. We also estimate the degree of interseismic coupling (defined in Section 4.0) on faults bounding the tectonic blocks, which has implications for seismic hazard assessment in New Zealand. Because the style of deformation varies significantly along strike of the plate boundary, with subduction, strike-slip, and oblique collision all represented, we are particularly interested in how the mode of slip partitioning changes along strike. For example, how do the roles of block rotation and faulting in slip partitioning vary along strike? We also discuss possible driving mechanisms for the observed block rotations in the South Island and explore the role of the migration of buoyant continental fragments in the evolution of the New Zealand plate boundary.

2 NEW ZEALAND'S TECTONIC SETTING

The Australian and Pacific plates converge obliquely at 48–39 mm yr^{-1} in New Zealand. Partly due to along strike variations

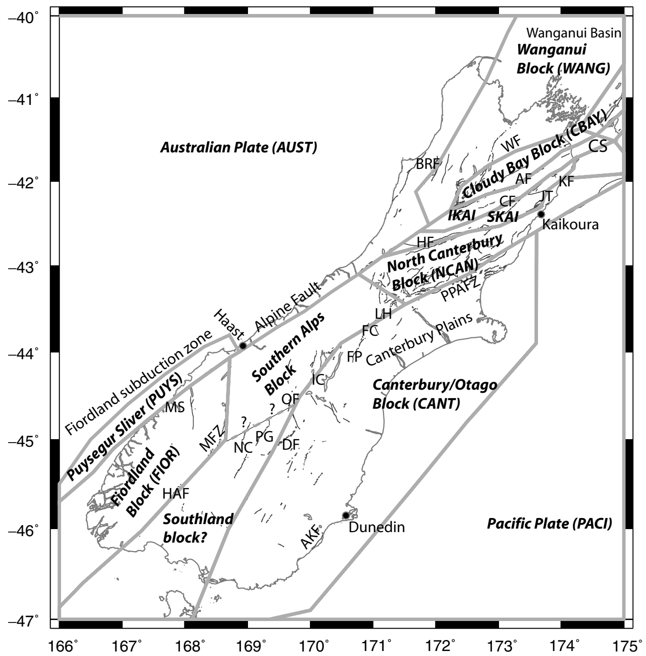

Figure 3. Tectonic block configuration used in this paper; heavy gray lines show block boundaries. Block names are shown in bold italics. Surface traces of known active faults (from GNS's active faults database; http://data.gns.cri.nz/af) are also shown as thin black lines (and some are labeled). Key to abbreviations: AF: Awatere Fault; AKF: Akatore Fault; BRF: Buller region faults; CS: Cook Strait; DF: Dunstan Fault; FC: Forest Creek Fault; FP; Fox Peak Fault; HAF: Haurako Fault; HF: Hope Fault; IC: Irishman's Creek Fault; IKAI: Inland Kaikoura block; JT: Jordan Thrust; KF: Kekerengu Fault; LH: Lake Heron Fault; MFZ: Moonlight Fault Zone; MS: Milford Sound; NC: Nevis-Cadrona Fault; OF: Ostler Fault; PG: Pisa-Grandview Fault; PPAFZ: Porter's Pass-Amberley Fault Zone; SKAI: Seaward Kaikoura block; WF: Wairau fault.

in the orientations of both the plate boundary and the direction of relative motion between the plates, the deformation takes on a larger strike-slip component southward. Accordingly, the style of deformation changes southwards from subduction of the Pacific Plate and backarc rifting in the North Island, to nearly pure strike-slip in the Marlborough region, to oblique convergence in the central South Island (causing formation of the central Southern Alps), and back to subduction of the Australian Plate at the Fiordland subduction zone in the southwestern South Island (Figs 1 and 3).

In the North Island, active tectonics are dominated by subduction of the Hikurangi Plateau (part of the Pacific Plate) beneath the eastern North Island at the Hikurangi Trough. North of 39°S, backarc rifting in the Taupo Volcanic Zone (TVZ) occurs (Fig. 1), while in the southern half of the North Island upper plate deformation is dominated by shortening and strike-slip. Subduction eventually ceases adjacent to where the thick continental crust of the Chatham Rise intersects the margin near 43°S. The subducted Pacific lithosphere underlies part of the northern South Island. An abrupt termination in intermediate depth seismicity beneath the Marlborough fault system (MFS) may mark the southern end of the subducting Pacific Plate (Anderson & Webb 1994), although the location of this slab edge is still debated (e.g. Anderson *et al.* 1994; Reyners & Robertson 2004).

The MFS in the northern South Island is dominated by four strike-slip faults (some with a component of reverse slip in northern Marlborough) that take up most of the relative plate motion: the Hope, Clarence, Awatere, and Wairau faults (e.g. Van Dissen & Yeats 1991, fig. 3). The Awatere (Little *et al.* 1998; Benson *et al.* 2001), Clarence (Kneupfer 1992; Nicol & Van Dissen 2002) and Wairau (Berryman *et al.* 1992; Zachariasen *et al.* 2006) faults each have Quaternary slip rates ranging from 4–8 mm yr^{-1}, while the Hope fault is slipping at ∼20 mm yr^{-1} (Cowan 1990; Van Dissen & Yeats 1991; Kneupfer 1992; Langridge & Berryman 2005). There is a general decrease in age of the Marlborough faults southwards (e.g. Yeats & Berryman 1987; Little & Jones 1998) that will be discussed later in connection with the evolution of the deforming zone (Section 6.3).

Slip on the MFS is eventually transferred onto the predominantly dextral strike-slip Alpine fault in the central South Island. The Alpine fault accommodates at least 70–75 per cent of the Pacific—Australia relative plate motion (e.g. Norris & Cooper 2001; Sutherland *et al.* 2006). A component of reverse slip on this fault is largely responsible for the growth of the Southern Alps. Paleoseismological studies in general indicate 27 ± 5 mm yr^{-1} of strike-slip and 5–10 mm yr^{-1} of dip-slip on the Alpine Fault (see review in Norris & Cooper 2001). The total dextral offset estimated on the Alpine Fault since its inception in the late Oligocene/early Miocene (e.g. Carter & Norris 1976; Cooper *et al.* 1987) is 480 km (reported by Wellman in 1949, quoted by Benson, 1952).

The Alpine Fault continues south into the Fiordland region and takes on a more purely strike-slip character (e.g. Hull & Berryman 1986; Sutherland & Norris 1995), with most of the activity on a western strand south of where where it goes offshore near Milford Sound (Barnes *et al.* 2005). Part of the Pacific/Australia convergence is accommodated on the Fiordland subduction zone, where the Australian Plate underthrusts the southwestern South Island. While several conceptual models for the 3-D configuration of this part of the plate boundary have been suggested (e.g. Lebrun *et al.* 2000; Reyners & Webb 2002; Malservisi *et al.* 2003), the Fiordland region is arguably the least well-understood section of the New Zealand plate boundary zone.

3 DATA USED IN THIS STUDY

3.1 GPS data analysis

The GPS data we use for the North Island and northern South Island are the same as those used by Wallace *et al.* (2004a). For the central and lower South Island, we use data from 15 regional GPS deformation surveys conducted between 1994 and 2004. The pre-1995 surveys in the Arthur's Pass region are not used because of coseismic and possible early postseismic deformation from the 1994 Arthur's Pass and 1995 Cass earthquakes (Arnadottir *et al.* 1995; Abercrombie *et al.* 2000). In each campaign, multiple sessions were observed where possible, with session lengths of 18–24 hr at most stations but as short as 7–8 hr in some cases. In the South Island, these shorter sessions occur only in some of the 1996 campaigns. The resulting network comprises about 800 stations distributed over the country, with the greatest density of GPS sites in the southern North Island (Fig. 2).

The GPS phase data from all surveys were processed by standard methods using Bernese software versions 3.5 through 4.2 (Rothacher & Mervart 1996; Beutler *et al.* 2001) to determine daily estimates of relative coordinates and their covariance matrices. Of more than 5000 station-days of data, about 3 per cent of station observations are rejected because they appear as outliers (residuals greater than 3 standard errors) in single-survey variation of coordinate solutions. Some poorly-determined station observations are rejected as a result of observing sessions significantly less than 7 hr. The processing methods used to obtain relative coordinates, station velocities, and their uncertainties, and to place the velocities into an Australia-fixed reference frame, are identical to those described by Wallace *et al.* (2004a) so are not repeated here.

3.2 Other data used

In addition to the GPS data discussed above, we use GPS velocities of geodetic sites on the Pacific and Australian plates (Beavan *et al.* 2002). These velocities help to establish an Australian Plate reference frame as well as providing a Pacific Plate velocity boundary condition for the kinematic modelling. GPS velocities from sites on the interior of the Pacific and Australian plates provide the best data bearing on the current kinematics of those plates, and the GPS-derived kinematics are reasonably consistent with longer-term plate motions obtained from seafloor spreading studies (DeMets *et al.* 1994; Sutherland 1995; Cande & Stock 2004). We also use a regional velocity solution (in the ITRF 2000 reference frame) that we submitted to the global strain-rate project (Holt *et al.* 2005). This velocity field includes a number of Pacific and Australian IGS (International GNSS Service) stations, together with New Zealand continuous and first-order campaign stations. Because of its nationwide coverage and connection to regional IGS sites, this velocity field improves the accuracy with which the various local campaign velocity solutions are rotated into the Australia-fixed frame.

Earthquake slip vector azimuths on faults in the region are from Anderson *et al.* (1993), Doser *et al.* (1999) and Reyners & Webb (2002) (Table 1). Estimates of long-term fault slip rates and azimuths from major faults in the South Island (largely from active fault studies; Table 1) provide constraints on the kinematics of deformation in the plate boundary zone. We also require that relative motion across a block boundary should occur within a range of directions consistent with geological observations. The geological slip azimuths and earthquake slip vector azimuths are treated as normally-distributed data, with 1σ uncertainties. In the case of fault slip rate estimates, where slip rates are often quoted as a range of values, we usually treat them as uniformly distributed between those minimum/maximum values with some uncertainty on either side of those values (see Appendix B in McCaffrey, 2005 for detailed descriptions of the fitting functions). We assume this uncertainty to be $\sim$25 per cent of the range of slip rates, in contrast to McCaffrey (2005) who assumes 50 per cent of the range in his study of western US block kinematics. In a few cases, we treat the geological slip rate data as a 'hard constraint', where a severe penalty is imposed if the model relative motion direction and rates fall outside the appropriate range of values (these data also have a uniform distribution within the range). We use hard constraints (e.g. for the Marlborough faults, see Section 5.3) in cases where the GPS velocities can be fit by a variety of kinematic models; in such situations we rely on the geological data to narrow the range of valid kinematic models. The hard constraints are intended to overcome the statistical dominance of the numerous GPS velocities on the parameter estimation. All slip azimuth and slip rate data used, and whether they are treated as Gaussian or uniformly distributed data, or as a hard constraint, are given in Table 1.

4 MODELLING APPROACH

Interseismic deformation in the New Zealand plate boundary zone is dominated by a number of factors, but primarily by interseismic coupling on faults and rotation of tectonic blocks (e.g. Walcott 1984; Beavan *et al.* 1999; Beavan & Haines 2001; Darby & Beavan 2001; Wallace *et al.* 2004a). To interpret the South Island GPS velocity field, we implement a method developed by McCaffrey (1995, 2002) that matches the GPS velocities with long-term rotations of tectonic blocks (represented here as spherical caps), and elastic strain due to coupling on block-bounding faults. The non-linear inversion applies simulated annealing to downhill simplex minimization (Press *et al.* 1989) to simultaneously estimate the angular velocities of elastic blocks and coupling coefficients (defined below) on block-bounding faults, to give the best fit to the GPS velocities, earthquake slip vectors, and geological fault slip rates and azimuths. We minimize data misfit, defined by the reduced chi-squared statistic (χ^2_n). The method also allows us to optimally rotate multiple GPS velocity solutions into a common reference frame. In our case, we rotate the New Zealand-derived GPS velocity fields (nine different solutions, discussed in Section 3.1), and the regional velocity solution that we submitted to the global strain rate project, into an Australian Plate reference frame. Of the 873 GPS velocities available for this study, we remove 55 (6 per cent) that are clearly inconsistent with those of neighbouring sites or have horizontal velocity uncertainties higher than 3 mm yr^{-1}.

We divide the South Island into multiple tectonic blocks based on the locations of known, active faults (Fig. 3). Surface traces compiled in Stirling *et al.* (2002) and fault dips from the relevant geological and seismological studies define block-bounding fault geometries. Faults are defined by an irregular grid of nodes that extends both along strike and down dip (Fig. 5). In some cases, where the spatial density of GPS data are not sufficient to discriminate between multiple, nearby faults, our block boundaries are chosen to approximate a zone of distributed deformation (e.g. the boundary between the Southern Alps/Southland and Canterbury/Otago blocks, and the Porter's Pass/Amberley Fault zone; Fig. 3). While there is evidence for very slow deformation on faults (that we do not define) in the interiors of some of the tectonic blocks, the rates of motion on them are generally too low ($\ll$1 mm yr^{-1}) to be detectable using GPS techniques. However, in cases where distributed deformation on faults within a block might be significant, we invert for additional parameters that describe uniform horizontal (permanent) strain rates within the block (e.g. Savage *et al.* 2001; McCaffrey 2005), which allows the blocks themselves to undergo permanent deformation. This is particularly helpful in the South Island, where there are areas of distributed active faulting scattered throughout our chosen tectonic blocks (e.g. Little 2004), whose overall rates of deformation may exceed 1 mm yr^{-1}. In reality, there could be numerous, small-scale tectonic blocks in the South Island; however, the spatial distribution and uncertainties of our GPS velocities do not warrant such a complex model.

The short-term (interseismic) site velocities within a few tens of kilometers of most faults are considerably less than the long-term velocities expected from the relative motion of the adjacent tectonic blocks. This slowing is due to elastic strain adjacent to the fault caused by the friction (sometimes called 'locking' or 'coupling') between the two sides of the fault. There is some controversy regarding how to describe this phenomenon and what it means (Lay & Schwartz 2004; Wang & Dixon 2004). For our purposes we refer to a purely kinematic quantity we call the 'coupling coefficient', ϕ, to describe the process whereby friction causes the fault to be stuck for long periods. If V is the long-term slip rate on the fault (over many earthquake cycles) and V_c the short-term creep rate (the steady displacement rate across the fault surface over a short time, which may vary spatially), then $\phi = 1 - V_c/V$. If $\phi = 0$ the fault is creeping at the full long-term slip rate and if $\phi = 1$ there is no creep in the interseismic period. We represent fault slip behaviour as somewhere between those two extremes. In the case where ϕ is neither 0 nor 1, one could interpret it as a spatial average of creeping and non-creeping patches (Scholz 1990; McCaffrey *et al.* 2000a; Lay & Schwartz 2004). 'ϕ' is sometimes referred to as 'interseismic coupling' or 'interplate coupling' by other authors. In the inversion, we estimate ϕ at a grid of pre-defined nodes on the block-bounding faults, allowing us to determine along-strike and down-dip variations in ϕ. Values of ϕ between the nodes are determined by bi-linear interpolation. ϕ may also vary as a function of time, but we consider it to be time-invariant over the ∼12 yr span of our GPS data.

The relative motion (slip) vector (V) on the faults is determined by the Euler vectors describing the motions of the blocks on either side of the fault. The slip rate deficit vector on the fault is the scalar coupling value ϕ multiplied by the relative motion vector V between the two blocks at a given fault point. The elastic contribution to the

Table 1. Slip vector and fault slip rate data used in the inversion.

Block pairs	Fault	Longitude	Latitude	Data type (see notes)	Slip rate/azi data used (mm yr^{-1} or °)	UNC	Modelled value (mm yr^{-1} or °)	Source (see notes below)
SKAI-NCAN	Hope	172.5	−42.57	**GSR/HC**	17–24		18.1	K88, K84, C89
SKAI-NCAN	Hope	173.47	−42.38	**GSR/HC**	18–36		18	VDY91
CBAY-IKAI	Awatere	173.86	−41.74	**GSR/HC**	4–8		5.7	B01
IKAI-SKAI	Clarence	173.0	−42.3	**GSR/HC**	4–8		5.3.	VDY91
IKAI-SKAI	Clarence	172.13	−42.59	**GSR/HC**	4–8		5.4	VDY91
WANG-CBAY	Wairau	172.8	−41.8	**GSR/UD**	3–6	0.8	3.4	VDY91
WANG-CBAY	Wairau	172.8	−41.8	**AZI EST/GD**	60	10	65	VDY91
WANG-CBAY	Wairau	173.64	−41.55	**GSR/UD**	3–6	0.8	4.0	VDY91
WANG-CBAY	Wairau	173.64	−41.55	**AZI EST/GD**	103	17	99	MARLSS
SKAI-NCAN	Hope	172.29	−42.6	**AZI EST/GD**	70	10	69	MARLSS
IKAI-CBAY	Awatere	172.81	−42.16	**AZI EST/GD**	242	12	241	MARLSS
IKAI-CBAY	Awatere	173.54	−41.89	**AZI EST/GD**	240	10	239	MARLSS
IKAI-SKAI	Clarence	171.74	−42.59	**AZI EST/GD**	70	10	80	MARLSS
NCAN-PACI	Offshore Kaikoura	173	−42.8	**AZI EST/GD**	130	50	93	OSSHORT
NCAN-PACI	Offshore Kaikoura	174.17	−42.34	**GSR EST/UD**	1–8	1.8	8.7	OSSHORT
NCAN-CANT	PPAFZ	172.0	−43.28	**GSR/HC**	2–7		6.9	PPAFZEST
NCAN-CANT	PPAFZ	172.0	−43.28	**AZI EST/GD**	70	30	97	PPAFZEST
CANT-PACI		172.5	−44.8	**GSR/UD**	0–1.5	0.3	1.3	OSSHORT
CANT-PACI		174	−44	**GSR/UD**	0–1.5	0.3	1.6	OSSHORT
CANT-PACI		170	−47	**GSR/UD**	0–1.5	0.3	2.6	OSSHORT
CANT-PACI		172.5	−44.8	**AZI EST/GD**	100	50	20	OSSHORT
SALP-CANT	EALPF	168.3	−46.6	**AZI EST/HC**	30–150		31	EALPFEST
SALP-CANT	EALPF	169.4	−45.13	**AZI EST/GD**	35	115	78	EALPFEST
SALP-CANT	EALPF	169.4	−45.13	**GSR EST/UD**	0.5–5	1.1	3.7	EALPFEST
SKAI-AUST	Alpine F.	171.47	−42.73	**GSR/UD/FP**	8.5–11.8	2	14.6	BE92
SKAI-AUST	Alpine F.	171.47	−42.73	**GSR/UD/SH**	5.4–6.4	1	1.9	BE92
AUST-SALP	Alpine F.	170.5	−43.2	**GSR/UD/FP**	23–35	3	31.4	W97/98
AUST-SALP	Alpine F.	170.5	−43.2	**GSR/UD/SH**	4–7	1	4.3	W97/98
AUST-SALP	Alpine F.	170.1	−43.38	**GSR/UD/FP**	22–34	3	31.4	CN94
AUST-SALP	Alpine F.	170.1	−43.38	**GSR/UD/SH**	5–6	1	4.5	CN94
AUST-SALP	Alpine F.	170.05	−43.45	**GSR/UD/FP**	22–32	2.5	31.4	NC97
AUST-SALP	Alpine F.	170.05	−43.45	**GSR/UD/SH**	3.5–8	1.2	4.5	NC97
PUYS-SALP	Alpine F.	169.1	−43.9	**GSR/UD/FP**	21–32	2.6	24.9	CN95, BE98
PUYS-SALP	Alpine F.	169.1	−43.9	**GSR/UD/SH**	0.1–2	0.2	1.1	CN95
PUYS-SALP	Alpine F.	169.08	−43.92	**GSR/UD/FP**	24–32	2	24.9	BE98
PUYS-SALP	Alpine F.	169.08	−43.92	**GSR/UD/SH**	1.5–3	0.5	1.1	BE98
PUYS-FIOR	Alpine F.	168.05	−44.33	**GSR/UD/FP**	20–32	3	23.9	SN95
PUYS-FIOR	Alpine F.	168.05	−44.33	**GSR/UD/SH**	1–2	0.3	2.0	SN95
PUYS-FIOR	Alpine F.	168.03	−44.42	**GSR/UD/FP**	19–33	3.5	23.9	HB86, SN95
PUYS-FIOR	Alpine F.	168.03	−44.42	**GSR/UD/SH**	0.1–1.0	1.0	2.1	HB86, SN95
AUST-PUYS	FIORSZ	165.03	−46.06	**EQSV/GD**	110	20	112	A93
PUYS-FIOR	Alpine F.	166.87	−45.1	**AZI EST/GD**	45	10	47	SS-SALPF
AUST-PUYS	FIOR SZ	165.03	−46.06	**EQSV/GD**	290	20	292	A93
AUST-FIOR	FIOR SZ	166.88	−45.27	**EQSV/GD**	229	10	244	A93
AUST-PUYS	FIOR SZ	167.45	−44.67	**EQSV/GD**	268	18	285	A93
CBAY-IKAI	Awatere	172.74	−42.32	**EQSV/GD**	235	10	242	A93
AUST-WANG	Buller	171.67	−41.90	**EQSV/GD**	297	10	300	A93
AUST-WANG	Buller	171.58	−41.89	**EQSV/GD**	302	10	302	A93
AUST-WANG	Buller	171.96	−41.76	**EQSV/GD**	291	10	297	A93

Table 1. (*Continued.*)

Block pairs	Fault	Longitude	Latitude	Data type (see notes)	Slip rate/azi data used (mm yr^{-1} or °)	UNC	Modelled value (mm yr^{-1} or °)	Source (see notes below)
IKAI-SKAI	Clarence	174.4	−41.63	**EQSV/GD**	254	15	235	A93
SKAI-NCAN	Hope	171.93	−42.79	**EQSV/GD**	244	10	249	D99
SKAI-NCAN	Hope	172.99	−42.48	**EQSV/GD**	244	12	250	D99
AUST-PUYS	FIORSZ	166.56	−45.11	**EQSV/GD**	289	10	288	R02

Notes: Key to Abbreviations: AZI: azimuth; HC; data treated as a hard constraint using a penalty function; EQSV: earthquake slip vector; GSR = geological slip rate; AZI EST: possible range of sense of motion across a fault system/block boundary; GD: data with uncertainties treated as a Gaussian distribution; UD: data range treated as a uniform distribution (see McCaffrey 2005, Appendix B for detailed discussion of UD and GD treatment); FP: Fault parallel component of slip rate used; SH; horizontal shortening component of slip rate used; UNC: data uncertainties used for GD and UD cases; K88: Kneupfer (1988); K84: Kneupfer (1984); C89: Cowan (1989); VDY91: Van Dissen & Yeats (1991); B01: Benson *et al.* (2001); Y98: Yetton *et al.* (1998); BE92: Berryman *et al.* (1992); W97/98: Wright *et al.* (1997), Wright (1998); CN94: Cooper & Norris (1994); NC97: Norris & Cooper (1997); CN95: Cooper & Norris (1995); BE98: Berryman *et al.* (1998); SN95: Sutherland (1995); HB86 = Hull & Berryman (1986); A93: Anderson *et al.* (1993); D99: Doser *et al.* (1999); R02 = Reyners & Webb (2002); MARLSS: a range of azimuths consistent with domination of strike-slip on the faults in the Marlborough Fault System; OSSHORT: consistent with observations of slow shortening offshore N. Canterbury (Barnes 1996); PPAFZ: Porters Pass/Amberley Fault Zone; PPAFZEST: rough estimates of azimuth and rate of strike-slip and shortening on the PPAFZ, consistent with work by Berryman (1979), Kneupfer (1992), Cowan *et al.* (1996) and Pettinga *et al.* (2001). Note that we have allowed for the possibility that the slip rate in the PPAFZ could be higher than the geological estimates (2–5 mm yr^{-1}), as the only published slip rate estimates available for the PPAFZ are for a few of the main faults within this zone. Thus, the total slip accommodated across the PPAFZ could be somewhat higher; EALPF = zone of active faults in the eastern foothills of the Southern Alps, including the Ostler, Irishman Creeks, and Fox Peak faults, among others; EALPFEST = rough GSR and AZI estimates for the Southern Alps' eastern foothills faults consistent with slow shortening and/or strike-slip observed on these features; FIORSZ: Fiordland subduction thrust. All GSR data shown are in mm yr^{-1}, and all EQSV and AZI EST are shown in degrees east of north for the first block relative to the second block. Key to block abbreviations: AUST: Australia; PACI: Pacific; SKAI: Seaward Kaikoura block; IKAI: Inland Kaikoura block; CBAY: Cloudy Bay block; NCAN: North Canterbury block; CANT: Canterbury/Otago block; SALP: Southern Alps/Southland block; FIOR: Fiordland block; PUYS: Puysegur block; WANG = Wanganui block.

velocity field from the fault slip rate deficit is calculated using a back-slip approach to elastic dislocation modelling (Savage 1983), using the formulations of Okada (1985) for surface displacements due to dislocations in an elastic, half-space. With this approach, the pre-defined geometry of the fault in the region where interseismic coupling occurs influences the inversion result greatly, making it important to define realistic fault geometries where coupling might occur. In contrast, assumptions made about the geometry of the fault at depths where it creeps aseismically do not have an influence on our results (e.g. we cannot differentiate whether or not the creeping portion of the fault might project at depth as a vertical shear zone versus flattening out on a mid-crustal detachment). We also impose the constraint that ϕ decreases monotonically down-dip from a value of one (full interseismic coupling) at the surface to zero at some depth, because terrestrial faults in New Zealand reveal no evidence for aseismic surface creep.

4.1 Tectonic block and fault configurations used for the South Island

In the northwestern South Island, the Wanganui block (discussed in Wallace *et al.* 2004a) also encompasses part of the southwestern North Island and the Wanganui Basin (Fig. 3). In the South Island, the western boundary of this block is defined by a distinctive seismic lineation through the Buller region associated with a zone of reverse faulting, and the eastern boundary is the Wairau Fault (WF). We also define blocks between: (1) the Wairau and Awatere faults (AF) (the 'Cloudy Bay block'), (2) the Awatere and Clarence faults (CF) (the 'Inland Kaikoura block'; IKAI) and (3) the Clarence and Hope faults (HF) (the 'Seaward Kaikoura block'; SKAI). Where the Hope Fault goes offshore near Kaikoura, most of its slip is transferred onto the Kekerengu Fault via the Jordan Thrust (JT; Van Dissen and Yeats, 1991). Based on this, we use the Kekerengu Fault (KF) as the major block-bounding fault north of where motion slows on the Hope Fault. The Hope and Kekerengu faults provide a northwestern boundary for a 'North Canterbury block' whose southeastern boundary projects roughly through the Porter's Pass/Amberley Fault Zone (PPAFZ). For this paper, we do not attempt to connect the Hope, Clarence, and Awatere faults with strike-slip faults in the southern North Island, hence the arbitrary tectonic block boundary between the North and South Island in our model (with the exception of the Wanganui block). It is presently unclear how and if these faults connect across Cook Strait (e.g. Carter *et al.* 1988). We use estimates from surface geological studies for the dips of the Marlborough faults to define the block-bounding fault geometries at depth.

The Marlborough faults merge with the Alpine Fault, which is the major block-bounding fault in the central South Island. To merge the Alpine and Marlborough faults together at depth in the structural model, and avoid overlapping fault segments, we truncate the Marlborough faults against the Alpine Fault where they intersect at the surface, and the truncated ends of the Marlborough faults follow the plane of the Alpine Fault at depth.

The central Alpine Fault is set to dip 45°–55° to the east, consistent with geological (Sibson *et al.* 1981) and seismological evidence (Davey *et al.* 1995; Kleffmann *et al.* 1998). In the central South Island, we consider the block to the west of the Alpine Fault to be part of the Australian Plate. It is possible that there is a small amount of plate boundary deformation just west of the central Alpine Fault (e.g. Rattenbury 1986); however, GPS sites west of the fault are insufficient in areal coverage to accurately resolve slow motion of a west coast block relative to the Australian Plate. The Quaternary slip rate on the Alpine Fault (estimated from active faulting studies) accounts for ∼75 per cent of Pacific/Australia relative motion (e.g. Norris & Cooper 2001); the remainder must be accommodated elsewhere in the South Island.

Active deformation in the eastern foothills of the central Southern Alps is characterized by oblique (dextral) contraction (Fig. 3; e.g. the Ostler (OF), Irishman Creek (IC), Fox Peak (FP), Forest Creek (FC), and Lake Heron (LH) faults; Van Dissen *et al.* 1994; Pettinga *et al.* 2001; Upton *et al.* 2004). To represent this deformation, we have chosen the eastern boundary of a 'Southern Alps block' to project roughly through this zone of active faults in the eastern foothills of the Southern Alps (Fig. 3). We use a single fault surface to represent these known discontinuous faults because the spatial density of GPS velocities is insufficient to discriminate slip on multiple nearby faults. Because we place the eastern boundary of the Southern Alps block on the eastern edge of the zone of active faults in the Southern Alps foothills, we choose our block-bounding fault to dip to the west (beneath the zone of faults) in order to better replicate this zone of deformation. The Alpine fault constitutes the western boundary of the Southern Alps block.

It is possible that a separate 'Southland block' exists to the south of the Southern Alps block, partly based on the distinct modes of deformation observed within these two regions. However, due to the sparsity of GPS data in Southland, and the lack of an obvious structure/zone of faults forming a boundary between the Southland and Southern Alps blocks, we treat these two blocks as a single composite block (Southern Alps/Southland block, or SALP block) for most of this study. However, in Section 5.5, we do address the possibility that substantial internal deformation of the Southern Alps crustal block occurs, and that the Southern Alps and Southland blocks are separate entities. The eastern boundary of the composite SALP block projects southwards through a zone ($\sim$75 km wide) of active reverse faults in central Otago, including the Nevis-Cadrona (NC), Pisa-Grandview (PG), and Dunstan Faults (DF) (e.g. Beanland & Barrow-Hurlbert 1988; Beanland & Berryman 1989, Fig. 3). Deformation on this part of the SALP boundary is very diffuse, and using the block approach we aim only to estimate the total rate of possible deformation across this zone.

We define the 'Canterbury/Otago block' (CANT) between the distributed zone of faulting in the foothills east of the Southern Alps, and a somewhat arbitrary block boundary just off the east coast of the South Island largely to test the possibility that the eastern South Island is not part of the Pacific Plate (e.g. Beavan *et al.* 2002). There is also geological evidence for slow convergent deformation near the east coast of the South Island (e.g. the Akatore Fault near Dunedin, Litchfield & Norris 2000, and along the edge of the Canterbury Plains, Barrell *et al.* 1996) and offshore of north Canterbury (e.g. Barnes 1996).

In the Fiordland region, we define a 'Fiordland block' (FIOR) which is bounded on the east by a zone of faults including the Hollyford and Haurako faults and the Moonlight Fault Zone (e.g. Norris & Carter 1982), and on the west by the southern portion of the Alpine Fault. The Alpine Fault becomes very steep and takes on nearly pure strike-slip motion in Fiordland and the region south of Haast (e.g. Berryman *et al.* 1992; Sutherland & Norris 1995). We also define a narrow crustal block, the 'Puysegur sliver' (PUYS) between the Fiordland subduction zone trench and the Alpine Fault offshore. We use the seismologically-defined configuration of the Fiordland subduction zone (e.g. Eberhart-Phillips & Reyners 2001) to define the subduction zone fault bounding the northwestern side of the Puysegur sliver.

5 INVERSION RESULTS

We present here the results for our best-fitting model based on the block boundaries described in Section 4 and the data in Section 3. In Section 5.5 we discuss an alternative model that may be more appropriate for the central Southern Alps region. We obtain an excellent fit to GPS velocities, geological fault slip rates and azimuths, and earthquake slip vectors in the South Island (Fig. 4; Table 1). In our best-fitting model the $\chi_n^2 = 1.17$, indicating that the data are fit at their level of uncertainty. We estimate 217 parameters (including 138 free parameters for angular velocities and fault coupling coefficients for the North Island; see Wallace *et al.* 2004a) using 818 horizontal GPS velocities (1636 observations), 30 earthquake slip vectors/fault slip azimuths, and 35 geological slip rates. The free parameters include: three rotation parameters for each of 13 tectonic blocks and 10 GPS datasets, three components of the strain rate tensor for two blocks (SALP and CHCH), and ϕ at 148 fault nodes. Our inversion results for the North Island are nearly the same as those presented in Wallace *et al.* (2004a) with the exception that the slip rate deficit distribution on the Hikurangi subduction interface has changed slightly due to the inclusion of additional northern South Island GPS velocities.

Most of the South Island blocks rotate about distant poles (Table 2) in contrast to the North Island where rotation occurs about poles located within a few hundred km of the blocks (Wallace *et al.* 2004a). All the faults we use as block boundaries appear to be coupled to some degree in the interseismic period (Fig. 5), consistent with the lack of evidence in New Zealand for faults with active surface creep. The elastic (Fig. 6) and long-term tectonic rotation (Fig. 7) velocity components are both important contributors to the GPS velocity field, highlighting the need for simultaneous inversion of block rotations and fault coupling parameters. It is also necessary to invert the entire New Zealand GPS dataset simultaneously (including the North Island), as the velocities in one region are influenced by faults from adjacent regions (for example, GPS site velocities in Marlborough are impacted by slip rate deficits on the nearby Hikurangi subduction zone and the Alpine Fault).

5.1 Fault slip rate deficit estimates

Substantial fault slip rate deficits are apparent on most major faults in the South Island; elastic effects from fault slip rate deficits influence the velocities at all GPS sites in the South Island (Figs 5 and 6). In Marlborough, we obtain ϕ values of 0.9 for the Awatere, and 0.6 for the Clarence fault to a depth of 13 km. The ϕ estimates on the Hope and Wairau faults are 0.8–0.9 down to 20 km depth, possibly indicating deeper coupling than the other Marlborough faults.

From seismological studies, the base of the seismogenic zone of the Alpine Fault between 42.5° and 44°S is estimated to be 10–12 km depth (e.g. Leitner *et al.* 2001), while previous geodetic studies indicate an interseismic coupling depth of only 5–8 km (Beavan *et al.* 1999). The previous geodetic estimates are based on a 2-D approach, assuming that slip rate deficits do not vary along strike of the fault and that GPS velocities in the central South Island are not influenced by slip rate deficits on other nearby faults (Beavan *et al.* 1999). Here, we allow along-strike variation of slip rate deficits on the Alpine Fault and influences from other nearby faults. Compared to Beavan *et al.* (1999), we obtain a deeper interseismic coupling depth estimate of 18 km ($\phi = 0.7$–0.85) for most of the Alpine Fault. However, since our ϕ values are less than 1.0 (full interseismic coupling), the equivalent depth of a fully locked fault may be less than 18 km (McCaffrey 2005), but still deeper than seismological estimates of 12 km. It should also be considered that seismological data gives us information about the depth to the base of the seismogenic zone, which may not be the same thing as the geodetically measured 'coupling depth', so drawing comparisons between 'seismological' and 'geodetic' coupling depths might not be appropriate. Our deeper coupling estimate may also be due to other factors, like ongoing deformation on structures <100 km to the east of the Alpine Fault (e.g. Cox & Findlay 1995; Little 2004), the implications of which

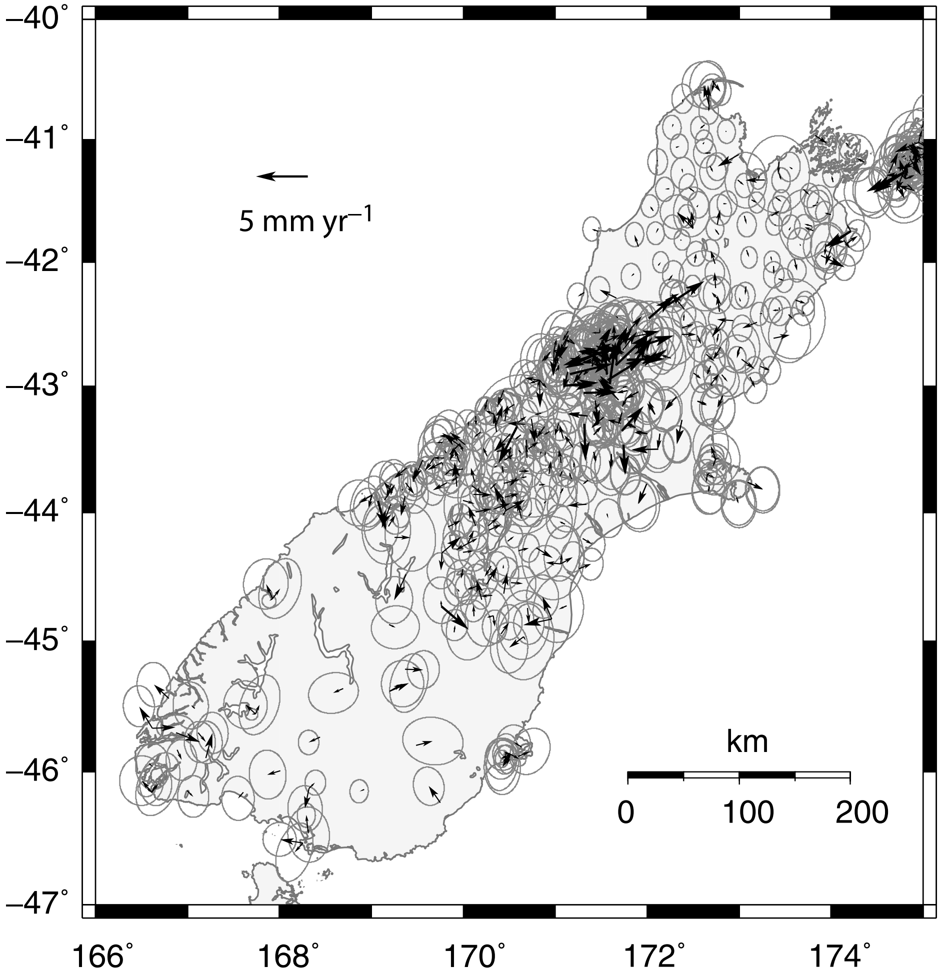

Figure 4. GPS velocity residuals for best-fitting block rotation/fault locking model with 95 per cent confidence data uncertainties (i.e. no contribution to the uncertainties from the model).

Table 2. Euler vectors for the tectonic blocks discussed in this study relative to the Australian Plate. Vertical axis rotation rates (V.A. rot. rate) at a point in the center of each block are shown in the last column. In all cases, Euler vectors are for the second plate relative to the first. e_{max}, e_{min}, and azimuth refer to the maximum and minimum standard errors of the uncertainty ellipse (in degrees), and the azimuth of the major axis, respectively. Negative rotation rates indicate clockwise motion. See Fig. 8 caption for key to block name abbreviations.

Plate pairs	Longitude	Latitude	Rate (° Myr^{-1})	e_{max}	e_{min}	Azimuth	V.A. rot. rate
AUST/WANG[a]	173.34	−39.67	−0.43 ± 0.09	0.43	0.28	234	−0.43
AUST/FIOR	252.07	−71.40	0.38 ± 0.33	60.8	1.7	11	0.27
AUST/SALP	228.33	−71.27	0.45 ± 0.3	40.1	1.2	168	0.35
AUST/CANT	183.60	−60.47	1.04 ± 0.08	1.8	0.2	119	1.00
AUST/NCAN	183.38	−56.84	1.07 ± 0.32	6.8	0.44	121	1.03
AUST/IKAI	175.19	−45.94	1.20 ± 0.44	2.44	0.39	116	1.20
AUST/SKAI	179.28	−51.81	0.73 ± 0.36	7.29	0.55	121	0.72
AUST/CLBY	173.41	−43.66	1.35 ± 0.57	1.03	0.22	98	1.35
AUST/PUYS	170.88	−33.69	−0.45 ± 0.42	12.98	1.54	259	−0.44
AUST/PACI[b]	184.19	−61.04	1.08 ± 0.004	0.37	0.17	82	1.03
AUST/AXIR[c]	174.33	−39.98	−2.80 ± 0.40	0.24	0.20	211	

[a]AUST/WANG pole shown here is slightly different from that of Wallace *et al.* (2004a) due to the inclusion of additional data in the northern South Island in this paper.
[b]From Beavan *et al.* (2002).
[c]AUST/AXIR pole is for the Axial Ranges block (relative to Australia) in the North Island. Wallace *et al.* (2004a) published an incorrect location for that pole in their Table 3, so here we publish the corrected pole location. Note that all slip rate calculations and diagrams in Wallace *et al.* (2004a) are based on the correct AUST/AXIR pole, the error is only in Table 3.

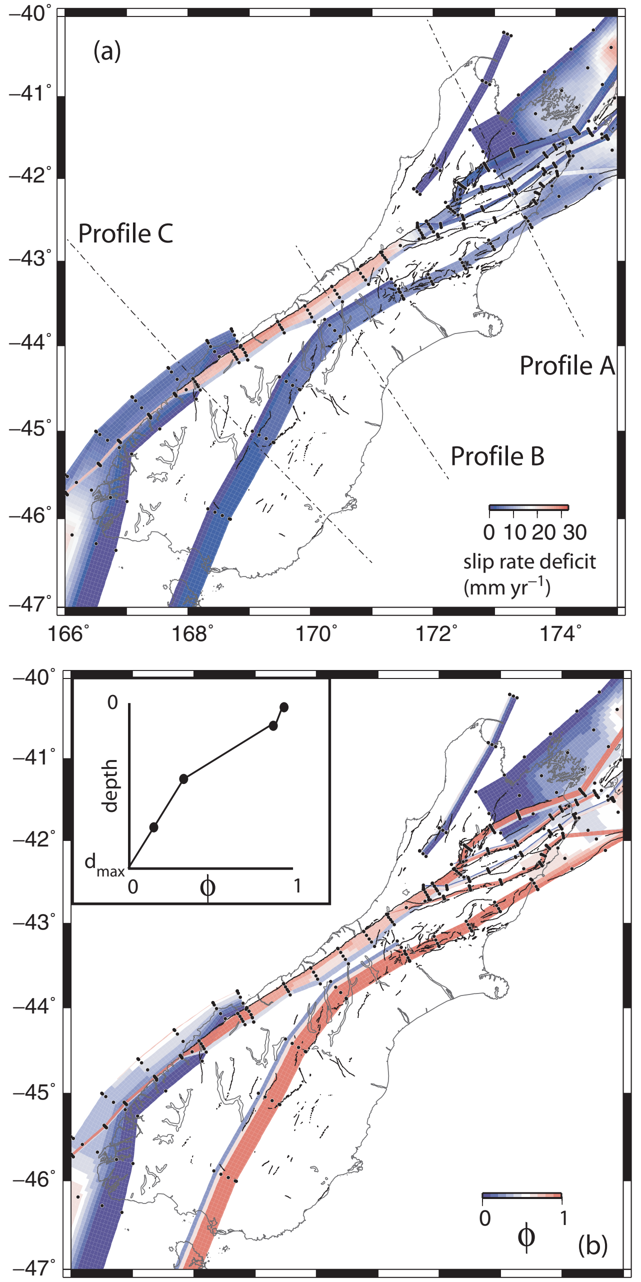

Figure 5. (a) Magnitudes of slip rate deficits (mm yr^{-1}) on block-bounding faults in the South Island. Dashed lines show locations of profiles in Fig. 11. (b) ϕ values (from 0 to 1) on the block bounding faults. The slip rate deficit is the scalar coupling coefficient (ϕ) multiplied by the relative block velocity. Locations of nodes used to specify 3-D fault geometries are shown as black dots that are projected vertically to the Earth's surface such that the width of the faults in the diagram reflects the dip of the fault (steeply dipping faults appear narrow, while shallowly dipping faults appear wide). Inset graph in (b) is a schematic of how ϕ might vary with depth, given our constraint that $\phi = 1$ at the surface, and ϕ must decrease in value down-dip to 0 at the deepest fault node ($d_{\max}$ = depth to deepest defined fault node). Black dots represent node locations along a hypothetical down-dip fault profile.

we discuss in detail in Section 5.5. For example, some of the shear strain that we interpret here as being due to deeper coupling on the Alpine Fault may instead be due to distributed dextral deformation within the Southern Alps.

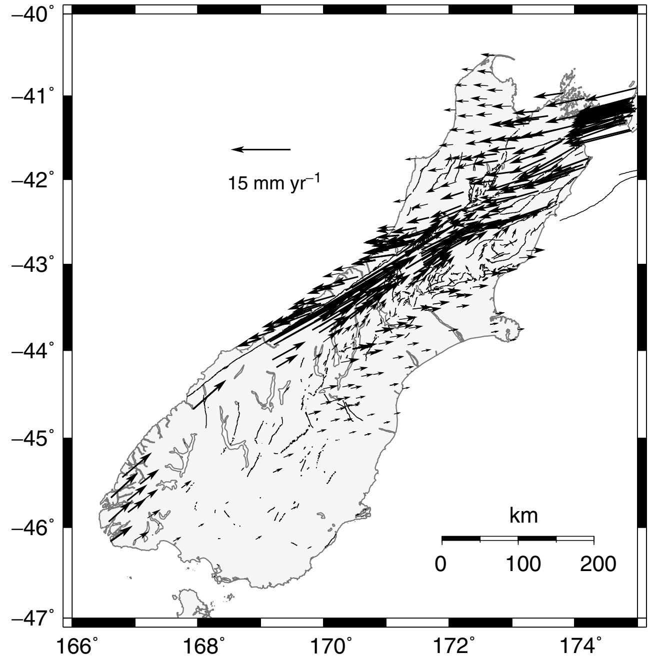

Figure 6. GPS site velocities predicted by the elastic strain component only, due to interseismic fault slip deficit rates calculated using the back-slip approach (i.e. rotations removed).

Our inversion results suggest some variation in the degree of coupling along strike of the Alpine Fault, between 42.5° and 44°S. For example, coupling on the central Alpine Fault from 1 to 18 km depth between 43° and 43.5°S appears to be slightly weaker ($\phi = 0.7$) than in surrounding segments ($\phi = 0.85$), which may indicate a relatively shallower coupling depth on the central portion of the Alpine Fault. The existence of a comparatively shallow seismogenic zone along the central Alpine Fault has been suggested previously based on elevated temperatures implying a thermally weakened crust (e.g. Allis *et al.* 1979; Koons 1987), and seismological evidence for high fluid pressures beneath the central Southern Alps (Stern *et al.* 2001).

We estimate full coupling down to 18 km depth for the Alpine Fault south of 44°S, indicating larger slip rate deficits for the southern half of the Alpine Fault (including the offshore portion) compared to further north. We also estimate high ϕ values along the Fiordland subduction zone, consistent with the occurrence of moderately large subduction earthquakes in recent times (e.g. Anderson *et al.* 1993; Doser *et al.* 1999; Reyners & Webb 2002; Reyners *et al.* 2003).

5.2 Possible internal strain of South Island tectonic blocks

To assess the possibility of distributed permanent strain east of the Alpine Fault in the CANT and SALP blocks, we invert for components of the horizontal strain rate tensor for these blocks in our best fitting model (Table 4). It is likely that some of the internal 'permanent' block strain that we estimate is actually elastic (due to coupling on faults inside the tectonic blocks); however, given the uncertainties in the GPS dataset we cannot differentiate between permanent deformation on aseismically slipping block interior faults versus interseismic coupling on these block interior faults. The improvement in fit to the data when we estimate strain rates in these blocks is not significant when compared to the elastic block assumption

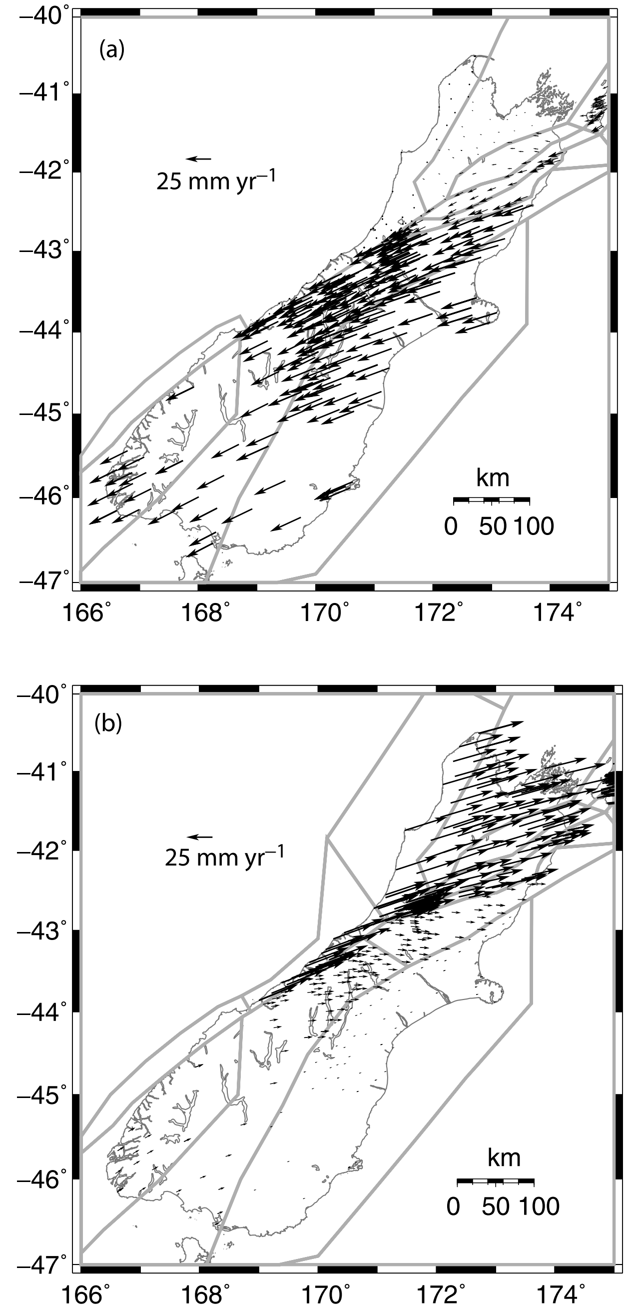

Figure 7. GPS site velocities predicted from long-term block rotations (i.e. short-term, elastic components removed), relative to (a) Australian Plate, (b) Pacific Plate.

(compare Scenario 3 with Scenario 1, Table 3). For CANT, we estimate a strain rate $\varepsilon_1 = -16.5 \pm 3.5$ nstrain/year oriented $-70^\circ \pm 8^\circ$, and the orthogonal $\varepsilon_2 = -2.8 \pm 1.7$ nstrain/year (contraction is negative) (Fig. 8). This strain rate corresponds to ∼2 mm yr^{-1} of permanent contraction of CANT in a WNW direction for a 125-km-wide block. Assuming incompressibility, this horizontal strain rate tensor results in 20 nstrain yr^{-1} of vertical strain which, for a 30 km thick crust, suggests 0.6 mm yr^{-1} of crustal thickening. If isostatically balanced, this crustal thickening would result in about 0.1 to 0.2 mm yr^{-1} of uplift. The SALP block has a residual internal strain rate of $\varepsilon_1 = -3.9 \pm 6.4$ nstrain/year oriented $22^\circ \pm 17^\circ$, and $\varepsilon_2 = 11.8 \pm 8.5$ nstrain/year (Fig. 8), corresponding to <1 mm yr^{-1} of permanent deformation over the 100 km wide block. However, as we demonstrate in Section 5.5, part of the GPS signal that we interpret as elastic strain from Alpine Fault coupling may instead be due to distributed deformation within the Southern Alps ∼0–100 km to the east of Alpine Fault. In this case, permanent strain of the SALP block may be larger than we estimate in the model discussed here.

For the other blocks, we do not formally solve for the components of the permanent strain rate tensor but instead calculate a residual strain rate from the velocity residuals for the best-fitting elastic block model (Table 4). In nearly all cases, the residual strain rates are small and marginally significant (due to high uncertainties), indicating that the data can be fit well by assuming that there is negligible internal deformation of the blocks. The one exception is the North Canterbury (NCAN) block, that has a residual strain rate of $\varepsilon_1 = -8.8 \pm 3.1$ nstrain/year, and $\varepsilon_2 = 19.7 \pm 8.1$ nstrain yr^{-1}, with ε_1 oriented $-83^\circ \pm 8^\circ$.

5.3 Block kinematics and fault slip rates in the Marlborough region

Due to elastic strain from slip rate deficits on the closely spaced Marlborough faults, it is difficult to estimate Marlborough fault slip rates uniquely with GPS data alone. The narrow width of the Marlborough fault bounded blocks (15–40 km wide) in the NW direction results in large uncertainties in the poles of rotation for the Marlborough blocks, particularly in the WNW–ESE (100°–120°) direction (Table 2). Geological data (Table 1) used in the inversion (as a hard constraint) are critical for resolving some of these parameters because, unlike GPS, they are not influenced by the elastic strain component.

In general, we obtain an excellent fit to the GPS velocities and geological fault slip rates and azimuths in the Marlborough region (Table 1, Figs 4 and 8). In the inversion we obtain ∼18 mm yr^{-1} right-lateral strike-slip on the Hope Fault, and 5.3, 5.7 and 3.5 mm yr^{-1} of right-lateral strike-slip for the Clarence, Awatere, and Wairau faults, respectively. These rates add up to 32.5 mm yr^{-1} of the predicted 41–42 mm yr^{-1} of Pacific-Australia relative plate motion. The remainder of the plate motion budget (8.5–9.5 mm yr^{-1}) is accommodated by shortening in the Buller region on the western boundary of the Wanganui block (1–2 mm yr^{-1}) and slip on faults within the PPAFZ (6.5–7.5 mm yr^{-1}) (Fig. 8). Our PPAFZ rate is nearly double that of previous geological estimates (3–5 mm yr^{-1}; e.g. Cowan *et al.* 1996; Howard *et al.* 2005). However, geological slip rates for faults in the PPAFZ have only been estimated for the major faults in the zone (e.g. the Porter's Pass Fault), while the PPAFZ is a complex, wide fault zone, composed of many faults that accommodate dextral transpression (e.g. Pettinga *et al.* 2001). Our GPS velocities indicate that approximately half of the total slip rate across the PPAFZ has been accounted for in geological studies, while the remaining 2–4 mm yr^{-1} of slip must occur on other uncharacterized or undiscovered faults within the PPAFZ. Where the PPAFZ projects offshore, we predict ∼8–9 mm yr^{-1} oblique (right-lateral) shortening. This combination of right-lateral strike-slip and shortening could be accommodated along the Kekerengu Bank, Te Rapa, and Kaikoura faults, among other active faults and folds observed in the offshore region (e.g. Barnes & Audru 1999). Very slow shortening between the Pacific Plate and the Canterbury/Otago block (∼1–2 mm yr^{-1}) offshore of the east coast of the South Island may accommodate some relative plate motion (Fig. 8; see also Beavan *et al.* 2002)

Table 3. Results of F-tests for independence of some South Island blocks.

Model	N_{data}	$N_{\text{parameters}}$	DOF	χ^2_n	No. of South Island blocks
(1) Best Model	1701	217	1484	1.17	10
(2) No coupling[a]	1636	69	1567	9.88	10
(3) No SALP, CANT strain	1701	211	1490	1.22	10
(4) One block[c]	1698	207	1491	1.34	8
(5) SALP = CANT[d]	1699	210	1489	1.34	9
(6) FIOR = SALP	1700	214	1486	1.16	9
(7) ESIL = PACI[b]	1693	201	1492	1.45	8
(8) SALP, CANT = PACI	1694	204	1490	1.44	9
(9) CANT = PACI	1696	211	1485	1.27	10
Comparison of models	F-test probability	Inference			
Is (1) better than (2)?	0.99	Yes			
Is (1) better than (3)?	0.79	Maybe			
Is (1) better than (4)?	0.99	Yes			
Is (1) better than (5)?	0.99	Yes			
Is (1) better than (6)?	0.43	No			
Is (1) better than (7)?	0.99	Yes			
Is (1) better than (8)?	0.99	Yes			
Is (1) better than (9)?	0.94	Probably			

See Fig. 8 caption for block name abbreviations. DOF: Degrees of freedom.
[a]The 'no coupling' model refers to the situation where block rotations only are allowed. Note that this model was done with GPS data only: no slip rates or slip azimuths were included in the inversion.
[b]This model assumes that the Fiordland, Southern Alps/Southland and Canterbury/Otago blocks are part of the Pacific Plate.
[c]The 'one block' model is where all the southeastern South Island blocks (SALP, CANT, FIOR) are considered to rotate as a single, large block.
[d]The SALP and CANT blocks rotate as a single block, but the block can strain uniformly.

indicated by active folding (with shortening rates of 0.1–0.9 mm yr^{-1}) offshore of North Canterbury (Barnes 1996).

Paleomagnetic and geological data indicate ~35° of clockwise rotation of tectonic blocks relative to the bounding Pacific and Australian plates in the northeastern part of Marlborough since 8 Ma (Fig. 9; Walcott *et al.* 1981; Mumme & Walcott 1985; Vickery & Lamb 1995; Little & Roberts 1997; Hall *et al.* 2004). By comparison, vertical axis rotation rates that we obtain for the Marlborough blocks (relative to the Australian Plate) are much lower (0.7–1.3° Myr^{-1}) and with the opposite sense of rotation (anti-clockwise). However, paleomagnetic samples younger than 8 Ma age from central and southern Marlborough exhibit negligible clockwise rotations and in some cases show anti-clockwise rotation (e.g. Roberts 1992; Vickery 1994; Little & Roberts 1997; Hall *et al.* 2004, Fig. 9). Based on paleomagnetic and structural geological evidence Vickery & Lamb (1995) and Little & Roberts (1997) suggest that the northeastern portion of Marlborough has undergone more rotation than its central and southwestern parts (Fig. 9). Therefore it is likely that our results mostly reflect what is occurring in central and southern Marlborough. In the northeastern corner there may be smaller, more rapidly rotating tectonic blocks (e.g. Little & Roberts 1997), similar to the North Island. The Marlborough blocks appear to be rotating about significantly different poles than the North Island blocks, implying that the central Marlborough and North Island blocks (with the exception of the Wanganui block, and possibly the northeastern corner of Marlborough) are not likely to be continuous, throughgoing tectonic blocks from the North through to the South Island.

5.4 Slip rates on the Alpine Fault

Overall, predicted slip rates on the Alpine Fault agree well with geological estimates (Fig. 8; Table 1). Rates on the far northern end (between 42.5°S and 43°S) gradually increase southward as slip is fed from the Marlborough faults onto the Alpine Fault (Berryman *et al.* 1992) (Fig. 8). Our kinematic model indicates nearly pure strike-slip motion on the Alpine Fault between the Awatere and Hope fault intersection points (Fig. 3), with rates of ~8 mm yr^{-1} on the Alpine Fault between the Awatere and Clarence fault intersections, and ~15 mm yr^{-1} slip rate on the Alpine Fault between the Clarence and Hope fault intersections. South of the intersection of the Hope and Alpine faults, the Alpine Fault takes on a much larger convergent component (~5 mm yr^{-1}) in addition to ~30–31 mm yr^{-1} right-lateral strike-slip, which is at the upper end of its geological strike-slip rate (27 ± 5 mm yr^{-1}) estimates. In view of the geological data, our 30–31 mm yr^{-1} strike-slip rate estimate may be too high; in Section 5.5 we discuss an alternative kinematic model which can fit the GPS velocities and produce a lower Alpine Fault slip rate. South of Haast (Fig. 8), movement on the Alpine Fault becomes nearly pure strike-slip and decreases to ~24 mm yr^{-1}, in agreement with geological observations (e.g. Hull & Berryman 1986; Sutherland & Norris 1995; Sutherland *et al.* 2006). The decrease in slip rate indicates that some of the slip from the central Alpine Fault is transferred onto the Fiordland subduction zone south of 44°S.

Our predicted convergent component of motion for the central Alpine Fault (43° to 44°S) is ~5 mm yr^{-1}, ~1–2 mm yr^{-1} less than average estimates from geological studies (e.g. Norris & Cooper 2001, and references therein). In our model (Fig. 8) the strike-slip component of motion for the central Alpine fault (south of its intersection with the Hope Fault at 43°S) accommodates ~80 per cent of Pacific-Australia relative motion parallel to the plate boundary strike while the convergent component accommodates ~50 per cent of the required component normal to the plate boundary.

5.5 Distributed deformation within the Southern Alps

The strike-slip component of motion that we estimate for the central Alpine Fault (31.0 ± 1.5 mm yr^{-1} between 43° and 44°S) is at

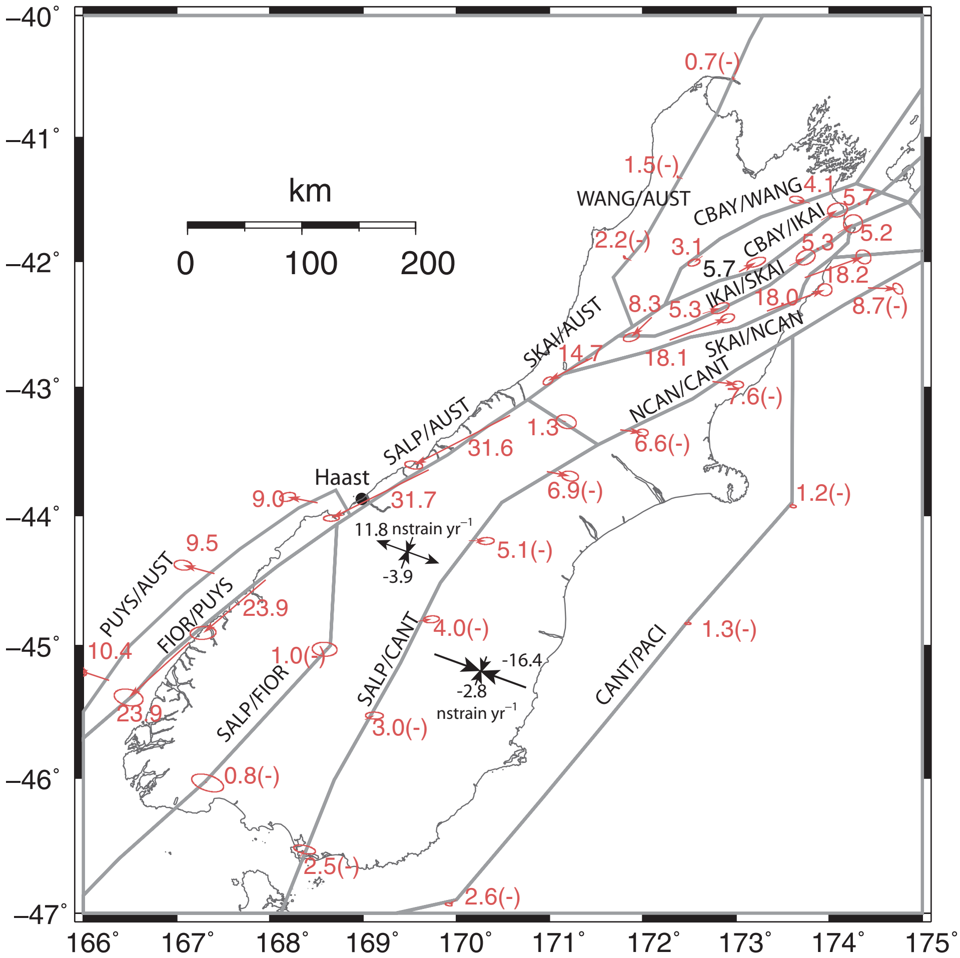

Figure 8. Predicted horizontal component of relative slip vectors across block boundaries (red arrows labeled with red numbers in mm yr^{-1}) for our best-fitting kinematic model, with 65 per cent confidence uncertainty ellipses. '+' and '−' signify extension and contraction, respectively. Each boundary is labeled with the two blocks involved in the relative motion with the vector indicating the motion of the first-named block relative to the second-named block. For example, at the boundary labeled 'SALP/CANT', the vectors show the Southern Alps/Southland (SALP) block movement relative to the Canterbury/Otago (CANT) block. Principal axes of the horizontal strain tensor we estimate for the SALP and CANT blocks (Table 4) are shown with strain rates in nstrain/year. Key to abbreviations: Australian Plate (AUST), Canterbury/Otago block (CANT), Cloudy Bay block (CBAY), Fiordland block (FIOR), Inland Kaikoura block (IKAI), North Canterbury block (NCAN), Pacific Plate (PACI), Puysegur sliver (PUYS), Southern Alps/Southland block (SALP), Seaward Kaikoura block (SKAI), and Wanganui block (WANG).

the high end for the average slip rates estimated from active fault studies of 27 ± 5 mm yr^{-1} (e.g. Norris & Cooper 2001, and references therein). Little (2004) suggested that dextral slip on numerous, closely spaced shear zones observed within the Alpine Fault hanging-wall can accommodate some of the plate boundary shear required in the central South Island. Structures observed in the now inactive Main Divide Fault Zone provide additional evidence that distributed deformation within the Southern Alps has occurred in the past (Cox & Findlay 1995). If significant distributed shear is accommodated on faults within 100 km east of the Alpine Fault, we may be incorrectly modelling this shear as elastic strain due to interseismic slip rate deficits on the Alpine Fault. This possible mis-identification of strain may explain why our best-fitting model suggests significantly deeper (∼18 km) interseismic coupling than the base of the seismogenic layer (∼12 km).

To test for the possibility of distributed deformation within the Southern Alps we divide the SALP block into separate Southern Alps and Southland blocks (Figs 3 and 10). We force the strike-slip rate on the central Alpine Fault to lie between 22 and 27 mm yr^{-1} and the total relative motion on the Southern Alps and Canterbury/Otago block boundary to be less than 7 mm yr^{-1}. These constraints effectively force the inversion to fit much of the GPS data in the central South Island by large permanent strain within the Southern Alps block. In this inversion, we are able to satisfy the slip rate constraints and GPS velocities in the Southern Alps block with a $\chi_n^2 = 1.63$ (Fig. 10) by permanent strain of the block with $\varepsilon_1 = -57.2 \pm 10.2$ nstrain/year, and $\varepsilon_2 = 65.3 \pm 7.6$ nstrain yr^{-1} with ε_1 oriented −70° ± 3°. The orientation of ε_1 is consistent with seismological estimates of principal horizontal shortening direction for the South Island of 110°–120° (Leitner *et al.* 2001). This model produces ∼5 mm yr^{-1} of permanent dextral deformation within the Southern Alps block (in good agreement with estimates of Little 2004) parallel to the Alpine Fault, accommodating ∼10–15 per cent of Pacific/Australia relative motion. Additionally, our estimate of the ϕ distribution on the Alpine fault changes markedly, with a much shallower coupling depth estimate (Fig. 10), more consistent with estimates of the maximum seismogenic depth in the Alpine Fault region from seismological studies (e.g. Leitner *et al.*

Table 4. Block principal strain rate estimates and 1σ uncertainties (10^{-9} yr^{-1}). Negative numbers signify contraction.

Block[a]	ε_1	ε_2	Azimuth[b] ε_1
FIOR[c]	-4.6 ± 6.2	0.2 ± 5.7	$-115° \pm 21°$
NCAN[c]	-8.8 ± 3.1	19.7 ± 8.1	$-83° \pm 8°$
SKAI[c]	-5.8 ± 11	8.1 ± 6	$21° \pm 19°$
IKAI[c]	-7.6 ± 16.1	33.8 ± 28	$-117° \pm 17°$
CBAY[c]	-12 ± 10.6	14 ± 19.2	$-80° \pm 23°$
WANG[c]	-0.7 ± 2.4	4.8 ± 2.4	$32° \pm 15°$
SALP[d]	-3.9 ± 6.4	11.8 ± 8.5	$22° \pm 17°$
CANT[d]	-16.4 ± 3.4	-2.8 ± 1.7	$-70° \pm 8°$
Southern Alps[e]	-57.2 ± 10.2	65.3 ± 7.6	$-70° \pm 3°$
CANT[e]	-16.6 ± 2.6	-0.42 ± 1.6	$-60° \pm 6°$

[a]See the caption for Fig. 8 for the key to block name abbreviations.
[b]Azimuth is in degrees east of north.
[c]These are strain rates estimated from the residual to the best-fitting model.
[d]Strain rates estimated in the inversion (SALP, CANT blocks only).
[e]Strain rate estimated in the test where the Southern Alps block undergoes higher strain to replicate distributed deformation within the Southern Alps (Section 5.5).

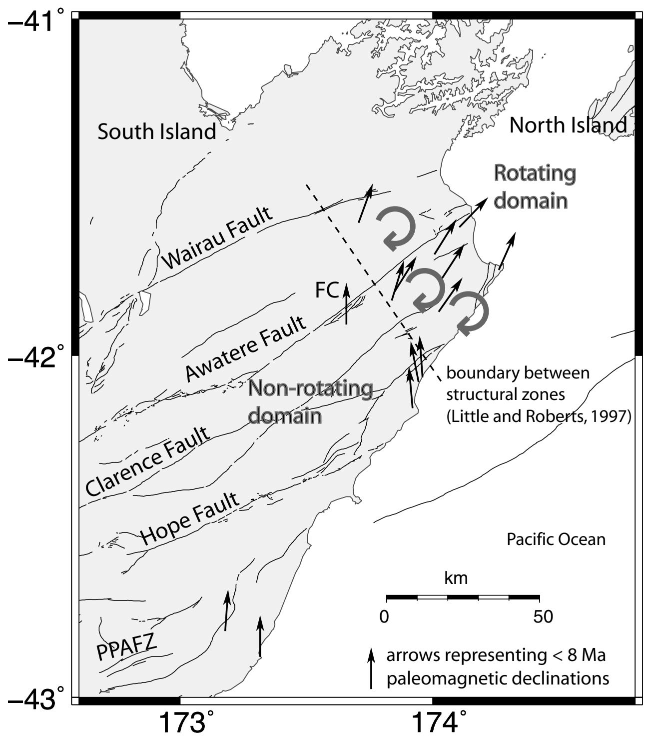

Figure 9. Summary of paleomagnetic evidence for rotations in Marlborough since 8 Ma. Azimuths of the straight black arrows indicate the amount of rotation (shown relative to north) since 8 Ma (from studies summarized in Hall *et al.* 2004). The dashed line refers to the change in structural grain documented by Little & Roberts (1997), which they suggest separates a 'rotating' domain in northeast Marlborough from a 'non-rotating' domain in central Marlborough. The circular arrows schematically represent clockwise rotation. FC: Fuschia Creek paleomagnetic locality; PPAFZ: Porter's Pass/Amberley Fault Zone.

2001). The fit to the data in this model ($\chi_n^2 = 1.63$) is not as good as our best-fitting model ($\chi_n^2 = 1.17$; Section 5.4), but this is largely due to greater misfit to the GPS velocities in the northern part of the Southern Alps block close to the MFS (Fig. 10; the remainder

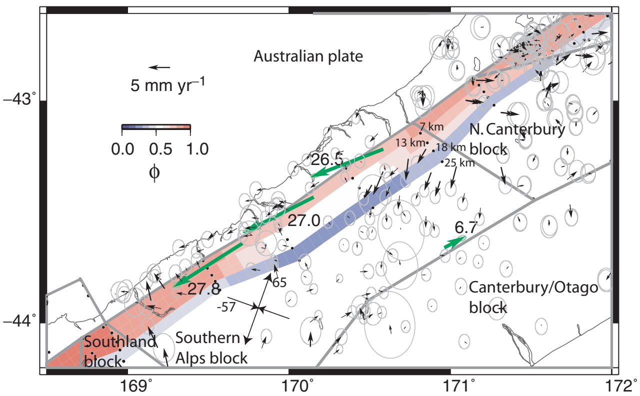

Figure 10. Tests for large permanent strain within the Southern Alps, using separate Southern Alps and Southland blocks. Thick, green arrows with rates (in mm yr^{-1}) beside them denote the relative motion across the block boundaries. Small black arrows with uncertainty ellipses are the velocity residuals relative to the model with large permanent strain rate within the Southern Alps block. Also shown are the interseismic coupling coefficients (ϕ) for the central Alpine Fault, and the principal axes of the estimated horizontal strain-rate tensor (in nstrain yr^{-1}) for the Southern Alps block. Depths of the Alpine Fault nodes are noted in km near the SALP and North Canterbury block boundary.

of the data are fit quite well). We suspect that a more complex permanent strain pattern (rather than simple uniform strain) within the Southern Alps would fit the data as well as the best-fitting model. Given the consistency with geological observations, we prefer this model of distributed deformation for the central Southern Alps over our 'best-fitting' model.

5.6 Deformation on faults in the eastern foothills of the Southern Alps

The kinematic model indicates 3–6 mm yr^{-1} of oblique (right-lateral) convergence on the SALP/CANT boundary in the eastern foothills of the Southern Alps (Fig. 8). This sense of motion and slip rate are largely consistent with thrust and right lateral strike-slip earthquake focal mechanisms and moment rates of events in that region, (e.g. Leitner *et al.* 2001; Berryman *et al.* 2002). The structures most likely to be accommodating this motion are the Ostler, Irishman Creek, Fox Peak, Forest Creek, and Lake Heron faults in the eastern foothills of the central Southern Alps, the Nevis-Cardrona, Pisa-Grandview, and Dunstan Faults, and related structures in central Otago (Fig. 3). In the inversion, we used a broad-slip rate estimate for this zone of faults (0.5–5 $\pm$ 1.1 mm yr^{-1}; Table 1) to allow for the possibility that geological studies have not found all of the active faults in that region. Most of the geological studies on this zone of faults have focused on estimating rates of contraction (<2 mm yr^{-1}, total), as the dextral slip rate on these faults is difficult to know. We estimate significant right lateral strike-slip (2–5 mm yr^{-1}) and contractional (2–5 mm yr^{-1}) components across this zone of faults, making the total slip rate (2.5–7 mm yr^{-1}) on the eastern foothills faults ~2–3 times higher than estimates from geological studies. It is likely that the geological studies have underestimated the dextral and possibly the contractional components of slip on known faults, and/or that there are other undiscovered active faults in the eastern foothills of the Southern Alps. A zone of elevated contractional strain within the eastern foothills of the Southern Alps (along the eastern boundary of the SALP block) is also seen in the GPS-derived strain-rate maps of Beavan & Haines

(2001), suggesting that contraction in this zone of faults is uniquely constrained by GPS data.

Our kinematic model also predicts 1–2 mm yr^{-1} of shortening (somewhat oblique) offshore between the CANT block and the Pacific Plate. This shortening is likely to be accommodated by active folding offshore of Canterbury (Barnes, 1996) and by reverse faults, such as the Akatore Fault near Dunedin (Fig. 3) that may accommodate 0.5–1 mm yr^{-1} of shortening, with a possible small component of right-lateral strike-slip (Litchfield & Norris 2000). Beavan *et al.* (2002) noted a ∼3 mm yr^{-1} ENE motion of GPS sites near Dunedin and Christchurch (OUSD and 5508) with respect to the Pacific Plate. This mismatch is explained in our kinematic model by 1–2 mm yr^{-1} of shortening on the CANT/PACI boundary and elastic strain due to interseismic slip rate deficits on the Alpine Fault and Marlborough fault system.

5.7 Fiordland region

Our kinematic model for the Fiordland region is constrained by GPS velocities, earthquake slip vectors on the Fiordland subduction zone (Anderson *et al.* 1993), fault slip azimuth estimates consistent with pure strike-slip on the offshore Alpine Fault (Barnes *et al.* 2005), and fault slip rate estimates from the on-land portion of the Alpine Fault (Hull & Berryman 1986; Sutherland & Norris 1995; Sutherland *et al.* 2006). We obtain a slip rate for the Alpine Fault offshore of Fiordland of 23.9 ± 2.5 mm yr^{-1}, and oblique convergence of 9–10 mm yr^{-1} at the Fiordland subduction boundary (∼88 per cent of PAC/AUS motion altogether). Like the suggestion of Norris & Cooper (2001), the geodetic data show that the convergent component of relative plate motion that occurs on the central Alpine Fault must be transferred offshore to the west of the southern Alpine Fault (south of Haast, where the sense of motion becomes purely strike-slip).

Barnes *et al.* (2002) use seismic reflection profiles to estimate 1–5 mm yr^{-1} of shortening perpendicular to the margin within the accretionary wedge in the Fiordland Basin. We obtain shortening rates perpendicular to the Fiordland subduction zone of 6.5–8 mm yr^{-1}, slightly higher than the upper end of their estimate. We also estimate that a component of dextral shear (3.5–6.0 mm yr^{-1}) must be accommodated within the Fiordland Basin thrust wedge, consistent with suggestions by Barnes *et al.* (2002) that 0–6 mm yr^{-1} of dextral shear is possible within the wedge. Their suggestion is partially based on the slight obliquity of earthquake slip vectors from events on the Fiordland subduction zone (seaward of the subduction zone's intersection with the Alpine Fault) with respect to the Fiordland subduction margin (Anderson *et al.* 1993). They also observe possible shutter ridges (and similar features) within the Fiordland Basin accretionary wedge that may indicate ongoing dextral shear.

We caution that the use of GPS velocities on their own cannot give insight into the details of how plate boundary deformation is partitioned between the southern Alpine Fault and the subduction zone offshore of Fiordland. The details of our kinematic model in this case require the use of earthquake slip vectors and fault slip rate estimates. Nor can we differentiate between the various scenarios that have been proposed for the cross-sectional development of the Fiordland region (e.g. Lebrun *et al.* 2000; Reyners & Webb 2002). However, the GPS velocities indicate that 85–90 per cent of Pacific/Australia relative motion must be accommodated offshore of Fiordland on the Alpine Fault and thrust faults. The remaining 10–15 per cent (3–6 mm yr^{-1}) probably occurs on reverse/oblique slip faults east of the Fiordland region (Fig. 8).

5.8 Statistical tests for South Island tectonic block independence

We conducted statistical tests of possible tectonic block configurations in the South Island (Table 3). For example, can the data distinguish an independent Canterbury/Otago block from the Southern Alps/Southland block and their motions from that of the Pacific Plate? Could the blocks in the eastern and southern South Island (CANT, SALP and FIOR blocks) constitute a single block? A test run in which all of the eastern and southern South Island blocks (SALP, CANT, and FIOR blocks) rotate as one block indicates that the data are not fit as well as alternative configurations (compare Scenario 4 to Scenarios 1, 5, and 6; Table 3). F-tests on the residual distributions suggest that the CANT and SALP blocks move independently (compare Scenario 5 to Scenario 1), indicating that some of the Australia-Pacific deformation not accommodated on the Alpine Fault must occur somewhere between the Southern Alps and the east coast. However, it is difficult to discern from the GPS velocities whether or not the FIOR block is independent of the SALP block (compare Scenario 6 to Scenario 1), as we get an equally good fit to either scenario. If deformation occurs between the FIOR and SALP blocks, it is likely to be very slow (e.g. Fig. 8).

Based on these tests, much of the South Island east of the Alpine Fault appears not to be part of the rigid Pacific Plate. A test in which all blocks east of the Alpine Fault (FIOR, SALP, CANT) are assumed to be part of the Pacific Plate (scenario 7) yields a significantly worse fit to the data than does the best-fitting model. The scenario where the SALP and CANT blocks are part of PACI (scenario 8) yields a similarly poor fit to the data. When the CANT block alone is forced to move with the Pacific Plate, the F-tests indicate that this scenario fits the data reasonably well, although still not as well as our best-fitting scenario (compare scenarios 1 and 9). This suggests that the CANT block is more similar to Pacific Plate motion than any other South Island block, but it is still likely (at 94 per cent probability) to be independent of the Pacific Plate.

6 DISCUSSION

6.1 Variations in the mode of slip partitioning in the South Island compared to the rest of New Zealand

Pacific/Australia relative motion is oriented obliquely relative to the variable strike of the New Zealand plate boundary zone. The variation in the plate boundary type, from subduction at the Hikurangi margin to nearly pure strike-slip in the Marlborough region, and oblique collision in the Southern Alps, causes large changes in the mode of slip partitioning along the New Zealand plate boundary.

In the North Island, the margin-parallel component of relative plate motion (assuming a 30° strike of the margin in the north, and a 40° strike at the southern end) is ∼28 mm yr^{-1} near 37.5°S, and ∼32 mm yr^{-1} near 41°S (Table 5; Beavan *et al.* 2002). Slip partitioning is known to occur in the North Island, as is evident from the orientation of subduction zone earthquake slip vectors perpendicular to the Hikurangi subduction margin (e.g. Webb & Anderson 1998), and from geological evidence for strike-slip faulting in the upper plate (e.g. Cashman *et al.* 1992). However, geological rates of strike-slip faulting reach only ∼6 mm yr^{-1} near 38°S and ∼21 mm yr^{-1} near 41°S (e.g. Beanland 1995; Van Dissen & Berryman 1996). Wallace *et al.* (2004a) demonstrate that clockwise rotation of the eastern North Island accommodates the remainder of the total margin-parallel component of Pacific-Australia relative motion. The net result of clockwise rotation of the eastern North

Table 5. Pacific-Australia relative motion at various points in New Zealand from Euler vector of Beavan *et al.* (2002).

Long.	Lat.	Total Rate (mm yr^{-1})	Vn (mm yr^{-1})	Ve (mm yr^{-1})	Strike-parallel rate (mm yr^{-1})	Strike-normal rate (mm yr^{-1})	Strike of margin used	Feature used for strike
167	−45	38.9	−17.2	−35	38.1	8.0	52	ALPF
168.86	−44	39.6	−15.3	−36.6	38.8	7.8	56	ALPF
169.91	−43.5	40	−14.3	−37.4	39.0	9.0	56	ALPF
170.77	−43.1	40.3	−13.5	−38	39.0	10.1	56	ALPF
179.6	−37.68	47.9	−4.6	−47.6	27.8	38.9	30	HIKM
179.36	−38.1	47.1	−4.9	−46.8	27.7	38.1	30	HIKM
178.73	−39.38	44.7	−5.5	−44.4	26.9	35.7	30	HIKM
178.41	−40.25	43.1	−5.8	−42.7	26.4	34.1	30	HIKM
177.69	−41.06	41.7	−6.6	−41.2	26.3	32.4	30	HIKM
177.69	−41.06	41.7	−6.6	−41.2	31.5	27.4	40	HIKM
174.85	−41.52	41.6	−9.4	−40.6	28.4	30.4	30	HIKM
173.36	−42.19	40.9	−10.9	−39.4	40.3	6.8	65	MFS
172.13	−42.59	40.6	−12.1	−38.8	40.2	5.4	65	MFS

Key to abbreviations: ALPF = Alpine Fault; HIKM = Hikurangi subduction margin; MFS = Marlborough fault system.

Island is extension in the TVZ (e.g. Villamor & Berryman 2001, and references therein), and shortening in the southern North Island, south of the TVZ (e.g. Melhuish *et al.* 1996; Nicol *et al.* 2002). Hence, slip partitioning in most of the North Island occurs largely by tectonic block rotation while strike-slip faulting plays a secondary role.

Though the margin-parallel rate of relative plate motion stays roughly the same along the Hikurangi margin, the margin-perpendicular component decreases significantly southwards (this decrease in proportion of the margin-normal component relative to margin-parallel causes the southward increase in obliquity; Table 5). Therefore, the southward increase in the observed rate of strike-slip faulting in the eastern North Island is not due to an along-strike change in Pacific/Australia relative plate motion. We argue instead that the greater strike-slip rate on faults in the southern North Island is due to the decreased role of rotation in accommodating the margin-parallel component of plate motion. Because the total change in tangential velocity across a rotating block is proportional to the block's width times the vertical axis spin rate, the southward decrease in the importance of rotation in the North Island is largely due to the narrower zone within which the plate boundary rotation occurs in the south (125 km) versus the north (200–250 km) (Fig. 11) and not due to slower rotation rates in the south.

In contrast to the North Island, block rotations in central and southern Marlborough region contribute very little to slip partitioning (Fig. 11). In this region, 97 per cent of AUS/PAC relative motion occurs via strike-slip on the Marlborough faults (including the PPAFZ). Slow shortening (1–2 mm yr^{-1}) in the Buller region accommodates the remaining 3 per cent. In Marlborough, the margin-parallel and perpendicular components of relative plate motion largely occur on separate structures (e.g. strike-slip in the MFS, and shortening in the Buller region), similar to 'classical' notions of slip partitioning (e.g. Fitch 1972; McCaffrey 1992). However, faults in the northern part of Marlborough probably accommodate a large amount of contraction as they have a more northerly strike (e.g. Jordan Thrust, Van Dissen & Yeats 1991; northern Awatere Fault, Little *et al.* 1998; London Hills Fault, Townsend & Little 1998; Clarence Fault, Nicol & Van Dissen 2002). Similarly, some faults in the PPAFZ accommodate dextral transpression. Paleomagnetic evidence for recent (<8 Ma) clockwise block rotations in northeastern Marlborough (e.g. Vickery & Lamb 1995; Little & Roberts 1997) suggest that rotation may also play a role in slip partitioning there, although we are unable to resolve with GPS whether or not these rotations still occur, presumably due to the small dimension of the region. If the paleomagnetically observed rotations continue today, it is likely that NE Marlborough is in a transitional zone between the North Island tectonic regime (characterized by rapid clockwise block rotations) and the nearly pure strike-slip observed in central Marlborough.

The Alpine Fault accommodates at least ~75 per cent of relative plate motion, and has components of convergence and strike-slip. Norris *et al.* (1990) and Norris & Cooper (1997) point out that in detail at the surface in the central Southern Alps, oblique slip is partitioned onto ENE trending thrust fault structures that are connected in a zig-zag pattern by WNW striking nearly pure strike-slip features. It is expected that these faults merge at depth where the slip is oblique. The remaining plate motion is distributed among strike-slip, oblique slip, and contractional faults to the east of the Alpine Fault.

In Fiordland, south of 44°S, ~63 per cent of the margin parallel component of relative plate motion occurs on the Alpine Fault (assuming a 50°–55° strike; Barnes *et al.* 2005), and 80–100 per cent of the convergent component of relative plate motion occurs on the Fiordland subduction thrust. Some oblique slip probably occurs at the Fiordland subduction zone (e.g. Barnes *et al.* 2002); we estimate up to 9–15 per cent of the margin parallel component could be accommodated within the Fiordland Basin thrust wedge (3.5–6.0 mm yr^{-1}). This is similar to the situation in Sumatra, where ~2/3 of margin-parallel plate motion occurs on the Sumatra Fault (strike-slip), while the remaining 1/3 occurs on the subduction thrust (McCaffrey *et al.* 2000b). The remaining 10–15 per cent of AUS/PAC motion (3–5 mm yr^{-1}) occurs as distributed deformation across the southern half of the South Island (east of the Alpine Fault).

Overall, in the North Island, the slip partitioning process is facilitated by block rotations, while in the South Island such rotations occur about more distant poles resulting in lower velocity gradients. Hence, relative plate motion in the South Island is accommodated more directly by faulting, some of which is quite oblique (e.g. the Alpine Fault).

6.2 Driving mechanisms for block rotations in New Zealand

Vertical axis rotation rates of all of the South Island tectonic blocks (including those in the Marlborough region) are similar in rate and sense (anti-clockwise, relative to the Australian Plate) to that of

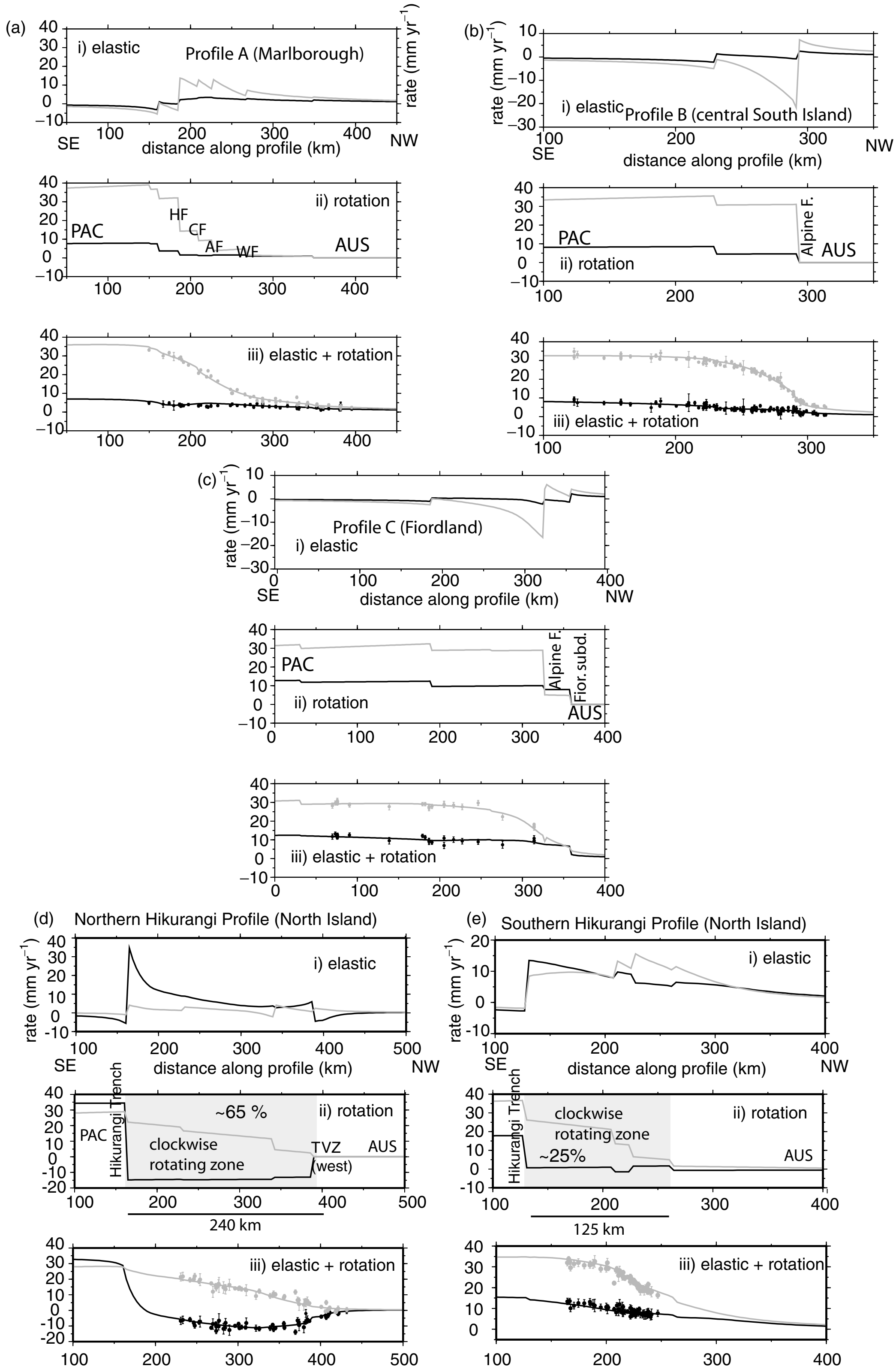

Figure 11. Profiles normal to the New Zealand plate boundary showing the margin-parallel (grey) and margin-perpendicular (black) components of the (i) elastic, (ii) rotational and (iii) combined elastic and rotational velocities. Observed velocities from GPS are projected onto the profiles as black and gray symbols. Locations of the three profile lines (a, b, c) from the South Island are shown in Fig. 5. Profile lines (d) and (e) from the North Island cross the northern (d) and southern (e) Hikurangi margin (Wallace *et al.* 2004a). Key features to note in the rotational component profiles are steps where there are faults and sloping lines between the faults where there are rotations. For the North Island profiles (d, e) the percentage of margin-parallel relative motion accommodated by rotation is given, and the grey shaded area indicates the zone where block rotations contribute to the margin parallel component of relative plate motion. In all cases the reference frame is the Australian Plate. AF; Awatere Fault; CF: Clarence Fault; HF: Hope Fault; WF: Wairau Fault; AUS: Australian Plate; PAC: Pacific Plate.

the Pacific Plate (Table 2). This implies that the kinematics of the South Island blocks are influenced more by the Pacific Plate than the Australian Plate. Likewise, in the western United States, vertical axis rotation rates relative to North America of tectonic blocks (caught up in the North America-Pacific plate boundary zone) are similar to that of the Pacific Plate (McCaffrey 2005). McCaffrey (2005) suggested that this occurs due to edge-forces being communicated across a block's boundaries (faults) to the neighbouring block, as opposed to the block rotations being driven by shear on the base of the blocks from a broadly deforming mantle substrate (e.g. the 'floating block' model, McKenzie & Jackson 1983; Lamb 1987) or ball-bearing type models (Schouten *et al.* 1993). Interestingly, the SALP block vertical axis rotation rate relative to Australia (0.35° Myr^{-1}, anti-clockwise) is smaller than the rotation rate of the CANT block relative to Australia (0.99° Myr^{-1}, anti-clockwise). This indicates that as the tectonic blocks get closer to the Australian Plate, the block kinematics may become progressively more influenced by edge forces arising from interaction with the Australian Plate. A comparable situation occurs in the western US, where the tectonic blocks closest to the North American Plate have vertical axis rotation rates more similar to that of the North American Plate (see fig. 14b in McCaffrey, 2005).

Some workers (e.g. Molnar *et al.* 1999; Stern *et al.* 2000) suggest that the mantle beneath the central South Island is undergoing dextral shear deformation over a zone up to 400 km wide, although others use a model of 'intracontinental subduction', where the Pacific Plate mantle is subducted beneath the Southern Alps, and deformation in the mantle occurs along a localized shear zone (e.g. Wellman 1979; Beaumont *et al.* 1996). If the eastern South Island crustal blocks (SALP, CANT blocks) were coupled to and sheared by a 400 km-wide zone of dextrally deforming mantle, they would be induced to rotate clockwise relative to the Pacific and Australian plates (e.g. the floating block model). Thus, the anti-clockwise rotation (relative to Australia) of the SALP and CANT blocks that we observe in geodetic data argues against a broad deforming zone in the mantle beneath the South Island, unless there is extreme decoupling between the crust and mantle. We note that the vertical axis rotation rate of the SALP block relative to the Pacific Plate is slightly clockwise (0.6° Myr^{-1}). However, for rotation of SALP to be consistent with the floating block model, it should exhibit clockwise rotation relative to *both* bounding plates (Australia and Pacific), and its vertical axis rotation rate should be somewhat greater than the relative rotation rate between the two bounding plates (here, $>1^\circ$ Myr^{-1}) (e.g. McCaffrey 2005). Finite-element modelling by Ellis *et al*. (GJI, in press, 2006) of GPS velocities from the central South Island indicate that if there is a deforming zone in the mantle beneath the central South Island, its width cannot be greater than $\sim$100 km. They found this to be the case even if the lower crust is very weak, as their modelling results suggest that deformation in the mantle is still likely to influence crustal deformation at the surface.

In northeastern Marlborough, paleomagnetic and geological studies (e.g. Vickery & Lamb 1995; Little & Roberts 1997) show that substantial clockwise rotations (up to 35°) have occurred in the last 8 Myr (Fig. 9). In the eastern North Island, paleomagnetic (e.g. Wright & Walcott 1986; Wilson & McGuire 1995) and geodetic data (Wallace *et al.* 2004a) indicate rapid clockwise rotations. Wallace *et al.* (2004a) suggest that the cause of this rotation is the influence on the subduction process of the southward increase in buoyancy of the subducting Pacific Plate. Although the 'floating block' model has been suggested to explain clockwise block rotations in northeastern Marlborough (Lamb 1988), we believe it is more likely that these clockwise rotations are due to subduction-related processes (Little & Roberts 1997; Reyners *et al.* 1997) similar to those that cause tectonic block rotations in the North Island (Wallace *et al.* 2004a). If so, northeast Marlborough may be connected to the North Island tectonic blocks across Cook Strait. However, the current distribution and accuracy of GPS velocities in northeastern Marlborough (Fig. 2) do not allow us to determine if these clockwise rotations are ongoing at present.

6.3 Major influences on the evolution of the New Zealand plate boundary zone

The Chatham Rise migrates southwest along the New Zealand plate boundary (relative to the Australian Plate) at $\sim$28–37 mm yr^{-1}, depending on the strike of the margin used (e.g. 30° strike of the Hikurangi Margin, or a 55° strike of the Alpine Fault) (Fig. 12). The southward migration of the Chatham Rise and Hikurangi Plateau (Fig. 1) permits southward propagation of the Hikurangi subduction zone relative to Australia. This propagation may in turn cause southward migration of the locus of activity in the MFS (and initiation of new faults in the MFS, such as the PPAFZ) as the Marlborough faults link up with the subduction zone (Berryman *et al.* 1992; Little & Roberts 1997). This southwards migration of subduction (and subsequent southeast-migrating faults in the MFS) is evidenced by the pattern of younger faults now found southeast of older faults

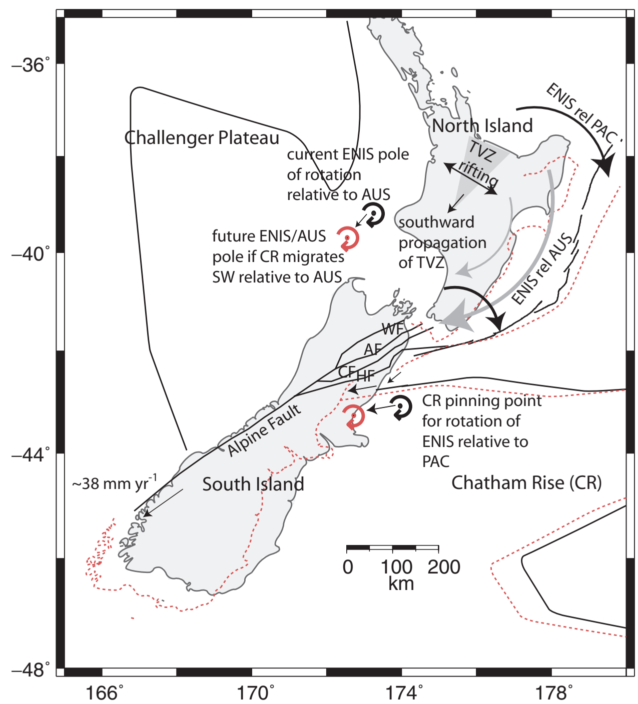

Figure 12. Schematic of the migration of the Chatham Rise, the New Zealand coastline and the TVZ relative to the Australian Plate over 2 Myr. The red dashed lines show the projected east coast of the North and South Island and the Chatham Rise (relative to a fixed Australian Plate) 2 Myr from now (ignoring coastal sedimentation and erosion). Small circular arrows (black = current, red = future) indicate poles of rotation of the eastern North Island (ENIS) relative to the Australian Plate (AUS) (poles located west of the central North Island), and poles of rotation for ENIS relative to the Pacific Plate (PAC), located near the Chatham Rise (CR). The large semi-circular arrows in the eastern North Island schematically depict its rotation relative to the Australian (grey arrows) and the Pacific (black arrows) plates. TVZ: Taupo Volcanic Zone; HF: Hope Fault; CF: Clarence Fault; AF: Awatere Fault; WF: Wairau Fault.

within the MFS, with the southeasternmost fault, the PPAFZ as the newest fault in the system (Cowan *et al.* 1996). Additionally, there is an accompanying diversion of slip away from the Alpine Fault onto the southward propagating MFS, effectively reducing the length of the rapidly slipping central portion of the Alpine Fault (e.g. Berryman *et al.* 1992). Following Little & Roberts (1997) we assume that southward propagation of the MFS and Hikurangi subduction zone relative to the Australian Plate follows the migration of the Chatham Rise along the New Zealand margin, and that the Alpine Fault/MFS intersection migrates southwest at a similar rate. Thus, the southernmost intersection of the Alpine Fault with the Marlborough faults 2 Myr from now will be approximately 56–74 km southwest of its current position. The average distance (measured along the Alpine Fault) between the intersection of each of the Marlborough faults with the Alpine Fault is ∼50 km. If the southwest migration of the Alpine Fault/MFS intersection occurs at a rate of 28–37 km Myr^{-1}, then a new fault within the Marlborough system should initiate roughly every 1.4–1.9 Myr. This timing is generally consistent with geological evidence for the initiation of Awatere Fault activity at 5.5–6.2 Ma (Little & Jones 1998), Clarence Fault initiation at 3 Ma (Browne 1992), and initiation of the Hope Fault at ∼1 Ma (Wood *et al.* 1994). The PPAFZ is currently in the process of establishing itself as a through-going fault zone (Cowan *et al.* 1996), ∼1 Ma after the Hope Fault.

The southward migration of the Chatham Rise and Hikurangi Plateau (relative to Australia) may also influence the tectonic evolution of the North Island. Wallace *et al.* (2004a) suggest that the rapid clockwise rotation of the eastern North Island occurs due to the change from collision of the buoyant Chatham Rise (a continental fragment) to subduction of the Hikurangi Plateau (buoyant oceanic plateau), and eventually, subduction of normal oceanic crust north of 36°S. This causes the eastern North Island tectonic blocks to pivot relative to the Pacific Plate about the Chatham Rise 'pinning point', where convergence is significantly slowed. Wallace *et al.* (2004a) suggest that this collision/subduction-induced rotation is the cause of backarc rifting in the TVZ. The locations of the poles of rotation for the eastern North Island blocks relative to Australia dictate the kinematics of rifting in the TVZ. Southward migration of the Chatham Rise relative to the Australian Plate may cause the poles of rotation of the North Island tectonic blocks (relative to the Australian Plate) to migrate southwards, following the Chatham Rise 'pinning point', leading to southward propagation of TVZ rifting (Fig. 12). Volcanological and geological evidence also suggests southward propagation of the TVZ (Gamble *et al.* 2003; Price *et al.* 2005; Villamor & Berryman 2006).

Analogous to the Hikurangi subduction zone, the Fiordland subduction zone propagates northwards (relative to the Pacific Plate; e.g. Walcott 1998) as the Challenger Plateau migrates northeast along the margin at a rate of ∼38 mm yr^{-1} (38 km Myr^{-1}). It is clear that the New Zealand plate boundary is continually evolving, and undergoing temporal changes largely driven by the presence and migration of buoyant crustal fragments (the Chatham Rise, Hikurangi Plateau and Challenger Plateau) along the plate boundary.

7 CONCLUSIONS

(1) We can fit the GPS velocity, geological slip rate and earthquake slip vector data within their uncertainties using a rotating, elastic block approach. Our kinematic model 'balances' the plate boundary velocity budget across the South Island of New Zealand, in that it accounts for how much deformation is required to satisfy Pacific/Australia relative plate motion.

(2) Most of the plate boundary deformation has been accounted for in geological studies, although there are regions where previous slip rate estimates may be too low. For example, in the Porter's Pass/Amberley fault zone, there may be 6–8 mm yr^{-1} of deformation compared to 3–5 mm yr^{-1} from geological studies (Cowan *et al.* 1996; Howard *et al.* 2005). Interpretation of GPS surface velocities suggests that slip rates on faults in the eastern foothills of the Southern Alps may be two to three times higher than geological estimates, particularly in the strike-slip component.

(3) The elastic, rotating block approach has enabled us to assess the interseismic slip rate deficits on some of the major faults in New Zealand, which can be incorporated into future seismic hazard models. We detect a shallower interseismic coupling depth on the central portion of the Alpine Fault in comparison to other areas of the fault, consistent with the suggestions of previous studies (e.g. Koons 1987; Stern *et al.* 2001).

(4) As an alternative to our 'best-fitting' model, we can also fit GPS velocities with ∼5 mm yr^{-1} of dextral deformation within the Southern Alps block <100 km to the east of the Alpine Fault; this could occur on a series of shear zones within the Southern Alps such as those described by Little (2004).

(5) The migration of buoyant continental masses (the Campbell Plateau and Chatham Rise) along the margin cause the plate boundary to continually evolve, and influence the development of the Marlborough fault system and the migration of the Fiordland and Hikurangi subduction zones. The change in orientation of PAC/AUS relative motion with respect to the orientation of the major plate boundary faults plays a secondary role in the variability of plate boundary environments observed in New Zealand.

ACKNOWLEDGMENTS

This work was funded by the Foundation for Research, Science and Technology (FRST), New Zealand. GPS data were collected by numerous individuals, principally from the Institute of Geological and Nuclear Sciences (now GNS Science), University of Otago, Dept. Of Survey and Land Information (now Land Information New Zealand), Oxford University, Victoria University of Wellington and occasional volunteers. McCaffrey's participation was supported by GNS Science and a sabbatical from Rensselaer Polytechnic Institute. This work benefited from discussions with Simon Cox, Susan Ellis, Nicola Litchfield, Tim Little, Andy Nicol, Martin Reyners, Russ Van Dissen and Pilar Villamor. Reviews of an earlier version of this manuscript by Simon Cox, Susan Ellis and Russ Van Dissen improved it. Detailed reviews by Tim Little and two anonymous reviewers improved the manuscript substantially. Many of the figures in this paper were made using Generic Mapping Tools software (Wessel & Smith 1995).

REFERENCES

Abercrombie, R.E., Webb, T.H., Robinson, R., McGinty, P.J., Mori, J.J. & Beavan, R.J., 2000. The enigma of the Arthur's Pass, New Zealand, earthquake 1. Reconciling a variety of data for an unusual earthquake, *J. geophys. Res.,* **105**(B7), 16 119–16 137.

Allis, R.G., Henley, R.W. & Carman, A.F., 1979. The thermal regime beneath the Southern Alps, in *The origin of the Southern Alps,* pp. 79–85, eds Walcott, R.I. & Cresswell, M.M., Wellington: Royal Society of New Zealand.

Anderson, H. & Webb, T., 1994. New Zealand seismicity: patterns revealed by the upgraded National Seismograph Network, *N.Z. J. Geol. and Geophys.,* **37,** 477–493.

Anderson, H., Webb, T. & Jackson, J., 1993. Focal mechanisms of large earthquakes in the South Island of New Zealand: implications for the accommodation of Pacific-Australia Plate motion, *Geophys. J. Int.,* **115,** 1032–1054.

Anderson, H. *et al.*, 1994. The 1968 May 23 Inangahua, New Zealand earthquake: An integrated geological, geodetic and seismological source model, *N.Z. J. Geol. and Geophys.,* **37,** 59–86.

Arnadottir, T., Beavan, J. & Pearson, C., 1995. Deformation associated with the 18 June 1994 Arthur's Pass earthquake, New Zealand, *N.Z. J. Geol. and Geophys.,* **38,** 553–558.

Barnes, P.M., 1996. Active folding of Pleistocene unconformities on the edge of the Australian-Pacific plate boundary zone, offshore North Canterbury, New Zealand, *Tectonics,* **17,** 534–557.

Barnes, P.M. & Audru, J.-C., 1999. Recognition of active strike-slip faulting from high-resolution marine seismic reflection profiles: Eastern Marlborough fault system, New Zealand, *G.S.A. Bull.,* **111**(4), 538–559.

Barnes, P.M., Davy, B., Sutherland, R. & Delteil, J., 2002. Frontal accretion and thrust wedge evolution under very oblique plate convergence, Fiordland Basin, New Zealand, *Basin Res.,* **14,** 439–466.

Barnes, P., Sutherland, R. & Delteil, J., 2005. Strike-slip structure and sedimentary basins of the southern Alpine Fault, Fiordland, New Zealand, *G.S.A. Bull.,* **117**(3/4), 411–435.

Barrell, D.J.A., Forsyth, P.J. & McSaveney, M.J., 1996. Quaternary geology of the Rangitata Fan, Canterbury Plains, New Zealand. *Institute of Geological & Nuclear Sciences science report 96/23,* Lower Hutt, New Zealand.

Beanland, S., 1995. The North Island dextral fault belt, Hikurangi subduction margin, New Zealand, *PhD thesis*, Victoria University of Wellington, New Zealand.

Beanland, S. & Barrow-Hurlbert, S.A., 1988. The Nevis-Cardrona Fault System, Central Otago, New Zealand: late Quaternary tectonics and structural development, *N.Z. J. Geol. and Geophys.,* **31**(3), 337–352.

Beanland, S. & Berryman, K.R., 1989. Style and episodicity of late Quaternary activity on the Pisa-Grandview Fault Zone, Central Otago, New Zealand, *N.Z. J. Geol. and Geophys.,* **32**(4), 451–461.

Beaumont, C., Kamp, P.J.J., Hamilton, J. & Fullsack, P., 1996. The continental collision zone, South Island, New Zealand: comparison of geodynamical models and observations, *J. geophys. Res.,* **101**(B2), 3333–3359.

Beavan, J. & Haines, J., 2001. Contemporary horizontal velocity and strain-rate fields of the Pacific-Australian plate boundary zone through New Zealand, *J. geophys. Res.,* **106**(B1), 741–770.

Beavan, J. *et al.*, 1999. Crustal deformation during 1994–1998 due to oblique continental collision in the central Southern Alps, New Zealand, and implications for seismic potential of the Alpine fault, *J. geophys. Res.,* **104**(B11), 25 233–25 255.

Beavan, J., Tregoning, P., Bevis, M., Kato, T. & Meertens, C., 2002. Motion and rigidity of the Pacific Plate and implications for plate boundary deformation, *J. geophys. Res.,* **107**(B10), doi: 10.1029/2001JB000282.

Benson, W.N., 1952. Meeting of the Geological Division of the Pacific Science Congress in New Zealand, February, 1949, *Interim Proceedings of the Geological Society of America 1950,* pp. 11–13.

Benson, A.M., Little, T.A., Van Dissen, R.J., Hill, N. & Townsend, D.B., 2001. Late Quaternary paleoseismic history and surface rupture characteristics of the eastern Awatere strike-slip fault, New Zealand, *G.S.A. Bull.,* **113**(8), 1079–1091.

Berryman, K., 1979. Active faulting and derived PHS directions in the South Island, New Zealand, in *The origin of the Southern Alps,* pp. 29–34, eds Walcott, R.I. & Cresswell, M.M., Wellington: Royal Society of NZ.

Berryman, K.R., Beanland, S., Cooper, A.F., Cutten, H.N., Norris, R.J. & Wood, P.R., 1992. The Alpine Fault, New Zealand, variation in Quaternary structural style and geomorphic express, *Annales Tectonicae,* **6,** 126–163.

Berryman, K.R., Cooper, A., Norris, R.J., Sutherland, R. & Villamor, P., 1998. Paleoseismic investigation of the Alpine Fault at Haast and Okuru, *Geological Society of NZ, Joint Annual Conference,: programme &abstracts*. Geological Society of NZ miscellaneous publication **101A,** 44.

Berryman, K.R., Stirling, M.W., Webb, T.H., Beavan, R.J. & Darby, D.J., 2002. Kinematics and strain at the Australia-Pacific plate boundary, South Island, New Zealand: integration of seismicity, earthquake geology, geodesy and plate motions, *Western Pacific AGU Meeting abstracts, Eos*, 83(22:supplement), **WP71**.

Beutler, G. *et al.*, 2001. Bernese GPS Software Version 4.2, eds Hugentobler, U., Schaer, S., Fridez, P., Astronomical Institute, University of Berne.

Browne, G.H., 1992. The northeastern portion of the Clarence Fault: tectonic implications for late Neogene evolution of Marlborough, New Zealand, *N.Z. J. Geol. and Geophys.,* **35,** 437–445.

Cande, S. & Stock, J., 2004. Pacific-Antarctic-Australia motion and the formation of the Macquarie Plate, *Geophys. J. Int.,* **157,** 399–414.

Carter, R.M. & Norris, R.J., 1976. Cainozoic history of southern New Zealand: an accord between geological observations and plate tectonic predictions, *Earth planet. Sci. Lett.,* **31,** 85–94.

Carter, L., Lewis, K.B. & Davey, F., 1988. Faults in Cook Strait and their bearing on the structure of central New Zealand, *N.Z. J. Geol. and Geophys.,* **31,** 431–446.

Cashman, S.M., Kelsey, H.M., Erdman, C.F., Cutten, H.N.C. & Berryman, K.R., 1992. Strain partitioning between structural domains in the forearc of the Hikurangi subduction zone, New Zealand, *Tectonics,* **11,** 242–257.

Cooper, A.F. & Norris, R.J., 1994. Anatomy, structural evolution, and slip rate of a plate-boundary thrust : The Alpine Fault at Gaunt Creek, Westland, New Zealand, *G. S. A. Bull.,* **106**(5), 627–633.

Cooper, A.F. & Norris, R.J., 1995. Displacement on the Alpine Fault at Haast River, South Westland, New Zealand, *N.Z. J. Geol. and Geophys.,* **38**(4), 509–514.

Cooper, A.F., Barreiro, B.A., Kimbrough, D.L. & Mattinson, J.M., 1987. Lamprophyre dyke intrusion and the age of the Alpine fault, New Zealand, *Geology,* **15,** 941–944.

Cowan, H.A., 1989. An evaluation of the Late Quaternary displacements and seismic hazard associated with the Hope and Kakapo Faults, Amuri District, North Canterbury, *PhD thesis*, Canterbury University, New Zealand.

Cowan, H.A., 1990. Late Quaternary displacements on the Hope Fault at Glynn Wye, North Canterbury, *N.Z. J. Geol. and Geophys.,* **33,** 285–293.

Cowan, H., Nicol, A. & Tonkin, P., 1996. A comparison of historical and paleoseismicity in a newly formed fault zone and a mature fault zone, North Canterbury, New Zealand, *J. geophys. Res.,* **101,** 6021–6036.

Cox, S.C. & Findlay, R.H., 1995. The Main Divide Fault Zone and its role in formation of the Southern Alps, *N.Z. J. Geol. and Geophys,* **38,** 489–499.

Darby, D.J. & Beavan, J., 2001. Evidence from GPS measurements for contemporary plate coupling on the southern Hikurangi subduction thrust and partitioning of strain in the upper plate, *J. geophys. Res.,* **106**(B12), 30 881–30 891.

Davey, F.J., Henyey, T., Kleffmann, S., Melhuish, A., Okaya, D., Stern, T.A. & Woodward, D.J., 1995. Crustal reflections from the Alpine Fault zone, South Island, New Zealand, *N.Z. J. Geol. and Geophys.,* **38,** 601–604.

DeMets, C., Gordon, R.G., Argus, D.F. & Stein, S., 1994. Effect of recent revisions to the geomagnetic reversal time scale on estimates of current plate motions, *Geophys. Res. Lett.,* **21,** 2191–2194.

Doser, D.I. & Webb, T., 2003. Source parameters of large historical (1917–1961) earthquakes, North Island, New Zealand, *Geophys. J. Int.,* **152,** 795–832.

Doser, D.I., Webb, T.H. & Maunder, D.E., 1999. Source parameters of large historic (1918–1962) earthquakes, South Island, New Zealand, *Geophys. J. Int.,* **139,** 769–794.

Eberhart-Phillips, D. & Reyners, M., 2001. A complex, young subduction zone imaged by three-dimensional seismic velocity, Fiordland, New Zealand, *Geophys. J. Int.,* **146,** 731–746.

Ellis, S., Beavan, J. & Eberhart-Phillips, D., 2006. Bounds on the width of mantle lithosphere flow derived from surface geodetic measurements: Application to central Southern Alps, New Zealand, *Geophys. J. Int.,* **166,** 403–417..

Fitch, T.J., 1972. Plate convergence, transcurrent faults, and internal deformation adjacent to Southeast Asia and the Western Pacific, *J. geophys. Res.,* **77,** 4432–4460.

Gamble, J.A., Price, R.C., Smith, I.E.M., McIntosh, W.C. & Dunbar, N.W., 2003. 40Ar/39Ar geochronology of magmatic activity, magma flux and hazards at Ruapehu volcano, Taupo Volcanic Zone, New Zealand, *J. Volc. geotherm. Res.,* **120,** 271–287.

Hall, L.S., Lamb, S.H. & Niocaill, C.M., 2004. Cenozoic distributed rotational deformation, South Island, New Zealand, *Tectonics,* **23**(2), doi:10.1029/2002TC001421.

Holt, W.E., Kreemer, C., Haines, A.J., Estey, L., Meertens, C., Blewitt, G. & Lavallée, D., 2005. Project helps constrain continental dynamics and seismic hazards, *EOS, Trans. Am. geophys. Un.,* **86,** 383–387.

Howard, M., Nicol, A., Campbell, J. & Pettinga, J.R., 2005. Holocene paleoearthquakes on the strike-slip Porters Pass Fault, Canterbury, New Zealand, *N.Z. J. Geol. and Geophys.,* **48,** 59–74.

Hull, A.G. & Berryman, K.R., 1986. Holocene tectonism in the region of the Alpine Fault at Lake McKerrow, Fiordland, New Zealand, in Recent Crustal Movements of the Pacific Region, pp. 317–331, eds. W.I. Reilly and B.E. Harford, *Royal Soc. NZ Bulletin,* **24,** New Zealand.

Kleffmann, S., Davey, F.J., Melhuish, A., Okaya, D. & Stern, T., 1998. Crustal structure in the central South Island, New Zealand, from the Lake Pukaki seismic experiment. *N.Z. J. Geol. and Geophys.,* **41**(1), 39–49.

Kneupfer, P.L.K., 1984. Tectonic geomorphology and present-day tectonics of the Alpine shear system, South Island, New Zealand, *PhD thesis*, 509 pp., University of Arizona, Tuscon.

Kneupfer, P.L.K., 1992. Temporal variations in latest Quaternary slip across the Australian-Pacific plate boundary, northeastern South Island, New Zealand, *Tectonics,* **11**(3), 449–464.

Kneupfer, P.L.K., 1988. Estimating ages of late Quaternary stream terraces from analysis of weathering rinds and soils, *G. S. A. Bull.,* **100,** 1224–1236.

Koons, P.O., 1987. Some thermal and mechanical consequences of rapid uplift: an example from the Southern Alps, New Zealand, *Earth planet. Sci. Lett.,* **86,** 307–319.

Lamb, S., 1987. A model for tectonic rotations about a vertical axis, *Earth planet. Sci. Lett.,* **84,** 75–86.

Lamb, S., 1988. Tectonic rotations about vertical axes during the last 4 Ma in part of the New Zealand plate boundary zone, *J. Structural Geology,* **10,** 875–893.

Langridge, R. & Berryman, K.R., 2005. Morphology and slip rate of the Hurunui section of the Hope Fault, South Island, New Zealand, *N.Z. J. Geol. and Geophys.,* **48,** 43–57.

Lay, T. & Schwartz, S.Y., 2004. comment on 'Coupling semantics and science in earthquake research', *EOS, Trans. Am. geophys. Un.,* **85**(36), 339–340.

Lebrun, J.-F., Lamarche, G. & Collot, J.-Y., 2000. Abrupt strike-slip fault to subduciton transition: the Alpine Fault-Puysegur trench connection, New Zealand, *Tectonics,* **19,** 688–706.

Leitner, B., Eberhart-Phillips, D., Anderson, H. & Nabelek, J.L., 2001. A focused look at the Alpine fault, New Zealand: Seismicity, focal mechanisms, and stress observations, *J. geophys. Res.,* **106**(2), 2193–2220, doi: 10.1029/2000JB900303.

Lensen, G.J., 1968. Analysis of progressive fault displacement during downcutting at the Branch River terraces, South Island, New Zealand, *G. S. A. Bull.,* **79,** 545–556.

Litchfield, N.J. & Norris, R.J., 2000. Holocene motion on the Akatore Fault, south Otago coast, New Zealand, *N.Z. J. Geol. and Geophys.,* **43**(3), 405–418.

Little, T.A. & Roberts, A.P., 1997. Distribution and mechanism of Neogene to present-day vertical axis rotations, Pacific-Australian plate boundary zone, South Island, New Zealand, *J. geophys. Res.,* **102**(B9), 20 447–20 468.

Little, T.A., 2004. Transpressive ductile flow and oblique ramping of lower crust in a two-sided orogen: Insight from quartz grain-shape fabrics near the Alpine fault, New Zealand, *Tectonics,* **23,** TC2013, doi:10.1029/2002TC001456.

Little, T.A. & Jones, A., 1998. Seven million years of strike-slip and related off-fault deformation, northeastern Marlborough fault system, South Island, New Zealand, *Tectonics,* **17**(2), 285–302.

Little, T.A., Grapes, R. & Berger, G.W., 1998. Late Quaternary strike slip on the eastern part of the Awatere fault, South Island, New Zealand, *G. S. A. Bull.,* **110**(2), 127–148.

Malservisi, R., Furlong, K.P. & Anderson, H., 2003. Dynamic uplift in a transpressional regime: numerical model of the subduction area of Fiordland, New Zealand, *Earth planet. Sci. Lett.,* **206,** 349–364.

McCaffrey, R., 1992. Oblique plate convergence, slip vectors, and forearc deformation, *J. geophys. Res.,* **97**(B6), 8905–8915.

McCaffrey, R., 1995. DEF-NODE users guide, Rensselaer Polytechnic Institute, Troy, New York, www.rpi.edu/~mccafr/defnode.

McCaffrey, R., 2002. Crustal block rotations and plate coupling, in *Plate Boundary Zones,* Vol. 30, pp. 100–122, eds Stein, S. & Freymueller, J., AGU Geodynamics Series.

McCaffrey, R., 2005. Block kinematics of the Pacific-North America plate boundary in the southwestern United States from inversion of GPS, seismological and geologic data, *J. geophys. Res.,* **110,** doi:10.1029/2004JB003307.

McCaffrey, R., Long, M.D., Goldfinger, C., Zwick, P.C., Nabelek, J.L., Johnson, C.K. & Smith, C., 2000a. Rotation and plate locking at the southern Cascadia subduction zone, *Geophys. Res. Lett.,* **27,** 3117–3120.

McCaffrey, R., Zwick, P.C., Bock, Y., Prawirodirdjo, L., Genrich, J.F., Stevens, C.W., Puntodewo, S.S.O. & Subaraya, C., 2000b. Strain partitioning during oblique plate convergence in northern Sumatra: Geodetic and seismologic constraints and numerical modeling, *J. geophys. Res.,* **105**(B12), 28 363–28 376.

McClusky, S., Bjornstad, S.C., Hager, B.H., King, R.W., Meade, B.J., Miller, M.M. & Monastero, F.C., 2001. Present day kinematics of the eastern California Shear zone from a geodetically constrained block model, *Geophys. Res. Lett.,* **28,** 3369–3372.

McKenzie, D.P. & Jackson, J.A., 1983. The relationship between strain rates, crustal thickening, paleomagnetism, finite strain, and fault movements within a deforming zone, *Earth planet. Sci. Lett.,* **65,** 182–202.

Meade, B.J. & Hager, B.H., 2005. Block models of crustal motion in southern California constrained by GPS measurements, *J. geophys. Res.,* **110,** B03403, doi:10.1029/2004JB003209.

Melhuish, A., Van Dissen, R. & Berryman, K., 1996. Mount Stewart-Halcombe Anticline: a look inside a growing fold in the Manawatu region, New Zealand, *N.Z. J. Geol. and Geophys.,* **39**(1), 123–133.

Molnar, P. *et al.*, 1999. Continuous deformation versus faulting through the continental lithosphere of New Zealand, *Science,* **286,** 516–519.

Morgan, W.J., 1968. Rises, trenches, great faults, and crustal blocks, *J. geophys. Res.,* **73,** 1959–1982.

Mumme, T.C. & Walcott, R.I., 1985. Paleomagnetic studies at Geophysics Division, 1980–1983, *Report/DSIR Geophysics Division 204,* Lower Hutt, New Zealand.

Nicol, A. & Van Dissen, R., 2002. Up-dip partitioning of displacement components on the oblique-slip Clarence Fault, New Zealand, *J. structural Geol.* **24,** 1521–1536.

Nicol, A., Van Dissen, R., Vella, P., Alloway, B. & Melhuish, A., 2002. Growth of contractional structures during the last 10 m.y. at the southern end of the emergent Hikurangi forearc basin, New Zealand, *N.Z. J. Geol. and Geophys.,* **45**(3), 365–385.

Norris, R.J., Koons, P.O. & Cooper, A.F., 1990. The obliquely-convergent plate boundary in the South Island of New Zealand: implications for ancient collision zones, *J. structural Geol.,* **12**(5–6), 715–725.

Norris, R.J. & Cooper, A.F., 1997. Erosional control on the structural evolution of a transpressional thrust complex on the Alpine Fault, New Zealand, *J. structural Geol.,* **19**(10), 1323–1342.

Norris, R.J. & Cooper, A.F., 2001. Late Quaternary slip rates and slip partitioning on the Alpine Fault, New Zealand, *J. structural Geol.,* **23,** 507–520.

Norris, R.J. & Carter, R.M., 1982. Fault-bounded blocks and their role in localising sedimentation and deformation adjacent to the Alpine Fault, Southern New Zealand, *Tectonophysics,* **87,** 11–23.

Okada, Y., 1985. Surface deformation to shear and tensile faults in a half-space, *Bull. seism. Soc. Am.,* **75,** 1135–1154.

Pettinga, J.R., Yetton, M.D., Van Dissen, R.J. & Downes, G.L., 2001. Earthquake source identification and characterisation for the Canterbury region, South Island, New Zealand. *Bull. of the N.Z. Soc. for Earthquake Engineering,* **34**(4), 282–317.

Press, W.H., Flannery, B.P., Teukolsky, S.A. & Vetterling, W.T., 1989. *Numerical Recipes,* Cambridge University Press, Cambridge.

Price, R.C., Gamble, J.A., Smith, I.E.M., Stewart, R.B., Eggins, S. & Wright, I.C., 2005. An integrated model for the temporal evolution of andesites and rhyolites and crustal development in New Zealand's North Island, *J. Volc. geotherm. Res.,* **140,** 1–24.

Rattenbury, M.S., 1986. Late low-angle thrusting and the Alpine Fault, central Westland, New Zealand. *N.Z. J. Geol. and Geophys.,* **29**(4), 437–446.

Reyners, M., Robinson, R. & McGinty, P., 1997. Plate coupling in the northern South Island and southernmost North Island, New Zealand, as illuminated by earthquake focal mechanisms, *J. geophys. Res.,* **102**(B7), 15 197–15 210.

Reyners, M. & Webb, T., 2002. Large earthquakes near Doubtful Sound, New Zealand, 1989–93, *N.Z. J. Geol. and Geophys.,* **45,** 109–120.

Reyners, M. & Robertson, E., 2004. Intermediate depth earthquakes beneath Nelson, New Zealand and the southwestern termination of the subducted Pacific plate, *Geophys. Res. Lett.,* **31,** doi: 10.1029/2003GL019201.

Reyners, M.E. *et al.*, 2003. The M_w 7.2 Fiordland earthquake of August 21, 2003: background and preliminary results, *Bull. of the N.Z. Soc. for Earthquake Engineering,* **36**(4), 233–248.

Roberts, A.P., 1992. Paleomagnetic constraints on the tectonic rotation of the Southern Hikurangi margin, New Zealand, *N.Z. J. Geol. and Geophys.,* **35,** 311–323.

Rothacher, M. & Mervart, L. (eds.), 1996. Documentation of the Bernese GPS Software Version 4.0, 418 pp, Astron. Inst., Univ. of Bern, Bern, Switzerland.

Savage, J.C., 1983. A dislocation model of strain accumulation and release at a subduction zone, *J. geophys. Res.,* **88,** 4984–4996.

Savage, J.C., Gan, W. & Svarc, J.L., 2001. Strain accumulation and rotation in the eastern California shear zone, *J. geophys. Res.,* **106,** 21 995–22 007.

Scholz, C., 1990. *The mechanics of earthquakes and faulting,* Cambridge Univ. Press, 439 pp.

Schouten, H., Kiltgord, K.D. & Gallo, D.G., 1993. Edge-driven microplate kinematics, *J. geophys. Res.,* **98,** 6689–6701.

Sibson, R.H., White, S.H. & Atkinson, B.K., 1981. Structure and distribution of fault rocks in the Alpine Fault Zone, New Zealand, *Geological Society of London Special Publication,* **9,** 197–210.

Stern, T., Molnar, P., Okaya, D. & Eberhart-Phillips, D., 2000. Teleseismic *P* wave delays and modes of shortening the mantle lithosphere beneath South Island, New Zealand, *J. geophys. Res.,* **105**(B9), 21 615–21 631.

Stern, T., Kleffmann, S., Okaya, D., Scherwath, M. & Bannister, S., 2001. Lower seismic wave speeds and enhanced fluid pressures beneath the Southern Alps, New Zealand, *Geology,* **29**(8), 679–682.

Stirling, M.W., McVerry, G.H. & Berryman, K.R., 2002. A new seismic hazard model for New Zealand, *Bull. seism. Soc. Am.,* **92,** 1878–1903.

Sutherland, R., 1995. The Australia-Pacific boundary and Cenozoic plate motions in the SW Pacific: Some constraints from Geosat data, *Tectonics,* **14,** 819–831.

Sutherland, R. & Norris, R.J., 1995. Late Quaternary displacement rate, paleoseismicity and geomorphic evolution of the Alpine fault: Evidence from near Hokuri Creek, south Westland, New Zealand, *N.Z. J. Geol. and Geophys.,* **38**(4), 431–450.

Sutherland, R., Berryman, K. & Norris, R., 2006. Quaternary slip rate and geomorphology of the Alpine Fault: implications for kinematics and seismic hazard in southwest New Zealand, *G.S.A. Bulletin,* **118**(3/4), 464–474.

Townsend, D.B. & Little, T.A., 1998. Pliocene-Quaternary deformation and near-surface strain near the eastern tip of the Clarence Fault, northeast Marlborough, New Zealand, *N.Z. J. Geol. and Geophys.,* **41,** 401–417.

Upton, P., Craw, D., James, Z. & Koons, P.O., 2004. Structure and late Cenozoic tectonics of the Southern Two Thumb Range, mid Canterbury, New Zealand, *N.Z. J. Geol. and Geophys.,* **47**(1), 141–153.

Van Dissen, R. & Berryman, K.R., 1996. Surface rupture earthquakes over the last ∼1000 years in the Wellington region, New Zealand, and implications for ground shaking hazard, *J. geophys. Res.,* **101**(B3), 5999–6019.

Van Dissen, R. & Yeats, R.S., 1991. Hope fault, Jordan thrust, and uplift of the Seaward Kaikoura Range, New Zealand, *Geology,* **19,** 393–396.

Van Dissen, R.J., Hull, A.G. & Read, S.A.L., 1994. Timing of some large Holocene earthquakes on the Ostler Fault, New Zealand, in *Proceedings of the Eighth International Symposium on Recent Crustal Movements (CRCM '93), Kobe, December 6–11, 1993,* pp. 381–386, Japan: Geodetic Society of Japan.

Vickery, S., 1994. Cenozoic deformation in a plate boundary zone, Marlborough, New Zealand, *D. Phil. Thesis,* Univ. Oxford, Oxford, UK.

Vickery, S. & Lamb, S., 1995. Large tectonic rotations since the Early Miocene in a convergent plate-boundary zone, South Island, New Zealand, *Earth planet. Sci. Lett.,* **136**(4), 3–59.

Villamor, P. & Berryman, K.R., 2001. A late Quaternary extension rate in the Taupo Volcanic Zone, New Zealand, derived from fault slip data, *N.Z. J. Geol. and Geophys.,* **44,** 243–269.

Villamor, P. & Berryman, K.R., 2006. Evolution of the southern termination of the Taupo Rift, New Zealand, *N.Z. J. Geol. and Geophys.,* **49,** 23–37.

Walcott, R.I., 1984. The kinematics of the plate boundary zone through New Zealand: a comparison of short- and long-term deformations, *Geophys. J. R. astr. Soc.,* **79,** 613–633.

Walcott, R.I., 1998. Modes of oblique compression: Late Cenozoic tectonics of the South Island of New Zealand, *Rev. geophys.,* **36**(1), 1–26.

Walcott, R.I., Christoffel, D.A. & Mumme, T.C., 1981. Bending within the axial tectonic belt of New Zealand in the last 9 Myr from paleomagnetic data, *Earth planet. Sci. Lett.,* **136,** 43–59.

Wallace, L.M., Beavan, R.J., McCaffrey, R. & Darby, D.J., 2004a. Subduction zone coupling and tectonic block rotations in the North Island, New Zealand., *J. geophy. Res.,* **109**(B12), B12406, doi:10.1029/2004JB003241.

Wallace, L.M. *et al.*, 2004b. GPS and seismological constraints on active tectonics and arc-continent collision in Papua New Guinea: Implications for mechanics of microplate rotations in a plate boundary zone, *J. geophys. Res.,* **109,** B05404, doi:10.1029/2003JB002481.

Wallace, L.M., McCaffrey, R., Beavan, J. & Ellis, S., 2005. Rapid microplate rotations and back-arc rifting at the transition between collision and subduction, *Geology,* **33**(11), 857–860, doi:10.1130/621834.1.

Wang, K. & Dixon, T., 2004. 'Coupling' semantics and science in earthquake research, *EOS, Trans. Am. geophys. Un.,* **85**(18), 180.

Webb, T.H. & Anderson, H., 1998. Focal mechanisms of large earthquakes in the North Island of New Zealand: slip partitioning at an oblique active margin, *Geophys. J. Int.,* **134,** 40–86.

Wellman, H.W., 1953. Data for the study of Recent and late Pleistocene faulting in the South Island of New Zealand, *N.Z. J. of Science and Technology,* **34B,** 270–288.

Wellman, H.W., 1979. An uplift map for the South Island of New Zealand and a model for uplift of the Southern Alps, in *The origin of the Southern Alps,* pp. 13–20, eds Walcott, R.I. & Cresswell, M.M., Wellington: Royal Society of New Zealand.

Wessel, P. & Smith, W.H.F., 1995. New version of the Generic Mapping Tools released, *EOS, Trans. Am. geophys. Un.,* **76,** F329.

Wilson, G.S. & McGuire, D.M., 1995. Distributed deformation due to coupling across a subduction thrust: mechanism of young tectonic rotation within the south Wanganui basin, New Zealand, *Geology,* **23**(7), 645–648.

Wood, R.A., Pettinga, J.R., Bannister, S., Lamarche, G. & McMorran, T.J., 1994. Structure of the Hanmer strike-slip basin, Hope fault, New Zealand, *G.S.A. Bull.,* **106,** 1459–1473.

Wright, C.A., 1998. Geology and paleoseismicity of the central Alpine Fault, New Zealand, *MSc thesis,* University of Otago, Dunedin, New Zealand.

Wright, I.C. & Walcott, R.I., 1986. Large tectonic rotation of part of New Zealand in the last 5 Ma, *Earth planet. Sci. Lett.,* **80,** 348–352.

Wright, C.A., Norris, R.J. & Cooper, A.F., 1997. Mapping of the central Alpine Fault, stage 1: Mikonui to Waitaha rivers, Westland. in Geological Society of NZ 1997 Annual Conference: 25–27 November, Wellington: programme and abstracts, Vol. 95A, p. 172, ed. Skinner, D.N.B., Geological Society of, N.Z. miscellaneous publication, Wellington, New Zealand.

Yeats, R.S. & Berryman, K.R., 1987. South Island, New Zealand and Transverse Ranges, California: a seismotectonic comparison, *Tectonics,* **6**(3), 363–376.

Yetton, M.D., Wells, A. & Traylen, N.J., 1998. The probabilities and consequences of the next Alpine Fault earthquake, *NZ Earthquake Commission, Research Report,* **95/193**.

Zachariasen, J., Berryman, K., Langridge, R., Prentice, C., Rymer, M., Stirling, M. & Villamor, P., 2006. Timing of late Holocene surface rupture of the Wairau Fault, Marlborough, New Zealand, *N.Z. J. Geol. and Geophys.,* **49,** 159–174.